Computational Mechanics
https://doi.org/10.1007/s00466-024-02583-0

ORIGINAL PAPER

A consistently linearized spectral stochastic finite element formulation for geometric nonlinear composite shells

Lukas Panther[1] · **Werner Wagner**[1] · **Steffen Freitag**[1]

Received: 25 September 2024 / Accepted: 29 November 2024

Abstract
Material and geometrical properties have a major influence on the structural behavior of geometric nonlinear shell structures. Therefore, uncertain structural parameters have to be considered within the context of stochastic structural analysis. The Monte Carlo simulation (MCS) is a widely used method for estimating statistical properties of the random structural response. Considering the computation time, however, this technique is challenging for complex finite element (FE) models and requires numerical efficient surrogate modelling approaches. An efficient way to propagate parametric uncertainties through complex models is the polynomial chaos expansion (PCE). Within the spectral stochastic finite element method (SFEM), the PCE is integrated into the FE formulation of structural elements. The application of the SFEM to geometrical nonlinear mechanical structures remains comparatively unexplored. In this paper, we present a geometric nonlinear spectral stochastic shell formulation. We use a layerwise formulation of the linear elastic material law to describe the behavior of composite materials. In order to apply Newton's method during the nonlinear solution procedure, all equations are consistently linearized to achieve a quadratic convergence in the iteration behavior. Two numerical examples show the applicability and efficiency of the presented spectral stochastic FE formulation. The SFEM results show a very good agreement compared to the results of the MCS. Special focus is set on the polynomial basis, which has a significant influence on the quality of the results, but also on the computational effort. We show, that the SFEM calculation provides a surrogate model, that can be used efficiently for further post-processing computations.

Keywords Nonlinear shell formulation · Spectral stochastic finite element method · Polynomial chaos expansion · Uncertainty quantification · Composite materials

1 Introduction

Components made of composite materials are becoming increasingly important in a wide range of technical applications. Due to their advantages, such as high strength combined with low specific weight, they are mainly used for lightweight constructions. Despite their outstanding properties, those structures can be at risk of stability due to their slenderness. In addition, thin-walled shell structures can be subjected to large deformations. These effects require the consideration of geometric nonlinearity in the numerical simulation.

The structural behavior of components made of these materials is significantly influenced by its material and geometrical parameters. However, these properties are affected by inherent randomness, which is also known as aleatoric uncertainty. The influence of aleatoric uncertain parameters on the structural behavior is investigated in the context of stochastic structural analysis. First, the sources of uncertainty have to be quantified. Uncertain material and geometrical parameters can be modeled as random variables or spatially correlated random fields. Subsequently, the random parameters are propagated through the computational model. Finally, the statistics of the quantities of interest, e.g., the maximal displacement or the maximal stress, can be calculated.

✉ Lukas Panther
lukas.panther@kit.edu

Werner Wagner
werner.wagner@kit.edu

Steffen Freitag
steffen.freitag@kit.edu

[1] Institute for Structural Analysis, Karlsruhe Institute of Technology (KIT), Kaiserstr. 12, 76131 Karlsruhe, Germany

Published online: 23 January 2025

The Monte Carlo simulation (MCS) is a widely used technique to estimate statistics such as mean value, variance and higher order moments of the random quantities of interest. Although this method is universal, it suffers from slow convergence behavior, see [1], which can be time consuming especially for complex computational models.

In this paper we adopt the approach of the spectral stochastic finite element method (SFEM), pioneered by [2] in the early 1990s. The key idea of the SFEM is the use of the polynomial chaos expansion (PCE), which was introduced by [3] for normal distributions. In [4, 5], the PCE has been extended to arbitrary probabilistic distributions. The PCE represents a random quantity in a polynomial basis spanned by orthogonal polynomials. In order to achieve optimal convergence of the PCE, the polynomial basis depends on the probability density function (PDF) of the random quantity.

Basically, it is distinguished between non-intrusive and intrusive methods for computing the coefficients of the PCE. In the last few years, least-square minimization in combination with adaptive methods, like least angle regression (LAR), developed by [6], has been established as an efficient non-intrusive method, see [7, 8]. They are referred to as sampling-based approaches, because they rely on repeated calls of the computational model for random realizations of the stochastic input parameters. Since the sampling procedure is the same as for the Monte Carlo simulation, the computational model can be used without any modifications. The intrusive approach, on the other hand, requires the governing equations to be modified, since they are projected onto the polynomial basis. Within the context of the SFEM, the uncertainty can be considered as an additional dimension of the degrees of freedom. Therefore, besides the spatial FE discretization, the stochastic space is discretized with the PCE. Special techniques are required for arithmetic operations such as multiplication of two polynomial chaos expansions, see [9]. An overview concerning implementation aspects of the SFEM can be found in [10–12].

The review papers [13, 14] provide an insight of the SFEM and its application in different research areas. A survey of programs in which the SFEM has been implemented is given by [15]. Up to now, there are many publications in which the SFEM is applied to various linear engineering problems. Originally, the method was developed by [2] and used in the field of linear elastic solid mechanics. In addition, the SFEM has been applied, e.g., to heat conduction [16, 17], transport in heterogeneous media [18], structural dynamics [19], diffusion problems [20] and flow simulations [5].

Within the field of linear solid mechanics, there are publications in which the SFEM is applied to shell formulations. In [21, 22] a spectral stochastic solid-like shell element is formulated in order to investigate fiber-metal laminates under the influence of spatially correlated random material parameters, such as the Young's modulus. A stochastic FE formulation of a triangular composite facet shell element is proposed in [23], where uncertainties in the material parameters and in the geometric properties such as the thickness of the shell are taken into account.

In contrast, the application of the SFEM for geometrical or material nonlinear problems is less developed so far. The consideration of problems with material nonlinearity, such as plasticity, in the context of the SFEM can be found in [24–27]. In [28], the method is used for uncertainty propagation in problems with finite deformations. A co-rotational geometric nonlinear stochastic beam formulation with finite rotations is proposed in [29]. In [30], the SFEM is formulated in the context of geometrical nonlinear problems. This involves investigations on the buckling behavior of a beam.

However, the SFEM has not been formulated in combination with general shell elements so far. Furthermore, there is no explicit derivation of the tangent stiffness matrix and residual available, which are required for an efficient implementation into a general finite element program. Also, the convergence behavior of the SFEM in the context of a geometrical nonlinear analysis is not yet considered. In this paper, we present a spectral stochastic finite element formulation for geometric nonlinear composite shells. The highlights of the paper can be summarized as follows:

- Derivation of a consistent formula for the tangent stiffness matrix and residual,
- Application of the assumed natural strain (ANS) interpolation [31, 32] for transverse shear in the context of the SFEM,
- Detailed illustrations of the consistently linearization in the context of the SFEM,
- Presentation of the seamless connection between the deterministic and stochastic formulas,
- Modular structure of the formulation, which allows a simple implementation into a finite element program,
- Application of an efficient and simple technique to reduce the size of the polynomial basis.

In Sect. 2 of the paper, the governing equations for geometric nonlinear shells are briefly described. The representation of stochastic quantities with the PCE and basic arithmetic operations with random variables are presented in Sect. 3. Subsequently, Sect. 4 illustrates the stochastic variational formulation of geometric nonlinear shells and the corresponding discretization in the stochastic dimension. This section includes as well the linearization of the random quantities. In Sect. 5, the spectral stochastic FE formulation for geometric nonlinear composite shells is derived. The developed stochastic FE formulation is applied to two numerical examples in Sect. 6. Appendices A–E contain supplementary material for intrusive operations within the PCE. Additional

informations for the developed shell formulation are provided in Appendices F–J.

2 Governing equations for geometric nonlinear shells

The shell theory is used for a general description of curved, thin-walled structures. The basic relationships briefly summarized in this section are based on shell formulations from [33–35]. The following assumptions and conditions are defined for the described shell concept:

- Reissner-Mindlin kinematics,
- Inextensible director field with $||\mathbf{d}|| = 1$,
- Moderate rotations with $|\beta_\alpha| < 8 - 10°,\ \alpha = 1, 2$,
- Use of convective coordinates $\left\{\xi^1, \xi^2, \xi^3 = \zeta\right\}$.

2.1 Kinematics

Let $\mathscr{B}$ be the three-dimensional Euclidean space occupied by the shell with the mid-surface Ω_0 and the shell thickness h. The position vector

$$\boldsymbol{\Phi}(\xi^1, \xi^2, \zeta) = \mathbf{X}(\xi^1, \xi^2) + \zeta\, \mathbf{D}(\xi^1, \xi^2) \tag{1}$$

with $||\mathbf{D}|| = 1$ is used to describe any point $P \in \mathscr{B}_0$ of the shell in the initial configuration. In a similar way, a point $P \in \mathscr{B}$ in the deformed shell space is defined by

$$\boldsymbol{\varphi}(\xi^1, \xi^2, \zeta) = \mathbf{x}(\xi^1, \xi^2) + \zeta\, \mathbf{d}(\xi^1, \xi^2) \tag{2}$$

with the thickness coordinate limited to $-h/2 \leq \zeta \leq +h/2$. The vectors $\mathbf{X}$ and $\mathbf{x}$ describe the shell mid-surface in the corresponding configuration. The displacement vector is introduced with

$$\mathbf{u} = \mathbf{x} - \mathbf{X}\,. \tag{3}$$

The deformed director $\mathbf{d}$ is used to specify the rotational behavior, see Fig. 1. Since we assume moderate rotations, $\mathbf{d}$ is given by

$$\mathbf{d} = \mathbf{D} + \boldsymbol{\beta} = \mathbf{A}_3 + (\beta_1\, \mathbf{A}_1 + \beta_2\, \mathbf{A}_2) \tag{4}$$

with the angles β_1 and β_2 related to the local tangential base system $\mathbf{A}_i$ with $i = 1, 2, 3$.

With the derivatives of the position vectors according to the convective coordinates, the components of the Green-Lagrangian strain tensor can be specified as

$$E_{\alpha\beta} = \frac{1}{2}\left(\boldsymbol{\varphi}_{,\alpha} \cdot \boldsymbol{\varphi}_{,\beta} - \boldsymbol{\Phi}_{,\alpha} \cdot \boldsymbol{\Phi}_{,\beta}\right), \quad \alpha, \beta = 1, 2\,. \tag{5}$$

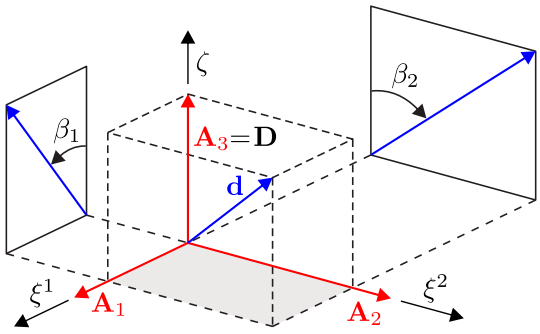

Fig. 1 Illustration of director $\mathbf{d}$ in the current configuration

In general, the nonlinear shell strains can be categorized into membrane strains

$$\varepsilon_{\alpha\beta} = \frac{1}{2}\left(\mathbf{x}_{,\alpha} \cdot \mathbf{x}_{,\beta} - \mathbf{X}_{,\alpha} \cdot \mathbf{X}_{,\beta}\right)\,, \tag{6}$$

curvatures

$$\kappa_{\alpha\beta} = \frac{1}{2}(\mathbf{x}_{,\alpha} \cdot \mathbf{d}_{,\beta} + \mathbf{x}_{,\beta} \cdot \mathbf{d}_{,\alpha} - \mathbf{X}_{,\alpha} \cdot \mathbf{D}_{,\beta} - \mathbf{X}_{,\beta} \cdot \mathbf{D}_{,\alpha}) \tag{7}$$

and shear strains

$$\gamma_{\alpha 3} = \mathbf{x}_{,\alpha} \cdot \mathbf{d} - \mathbf{X}_{,\alpha} \cdot \mathbf{D}\,. \tag{8}$$

Furthermore they can be arranged in the vector

$$\boldsymbol{\varepsilon} = \left[\varepsilon_{11}, \varepsilon_{22}, 2\varepsilon_{12}, \kappa_{11}, \kappa_{22}, 2\kappa_{12}, \gamma_{13}, \gamma_{23}\right]^T\,. \tag{9}$$

Based on the kinematic assumptions, the shell strains can be specified in terms of the local displacements and rotations

$$\boldsymbol{\varepsilon} = \begin{bmatrix} u_{1,1} + \frac{1}{2}\left(u_{1,1}^2 + u_{2,1}^2 + u_{3,1}^2\right) \\ u_{2,2} + \frac{1}{2}\left(u_{1,2}^2 + u_{2,2}^2 + u_{3,2}^2\right) \\ u_{1,2} + u_{2,1} + u_{1,1}u_{1,2} + u_{2,1}u_{2,2} + u_{3,1}u_{3,2} \\ \beta_{1,1} \\ \beta_{2,2} \\ \beta_{1,2} + \beta_{2,1} \\ \beta_1 + u_{3,1} \\ \beta_2 + u_{3,2} \end{bmatrix}\,. \tag{10}$$

$E_{33} = 0$ applies to the thickness strain, which is a consequence of the inextensible director field. The restriction to moderate rotations causes nonlinear components to occur only in the membrane strains. All displacements and rotations in Eq. (10) are shown in Fig. 2.

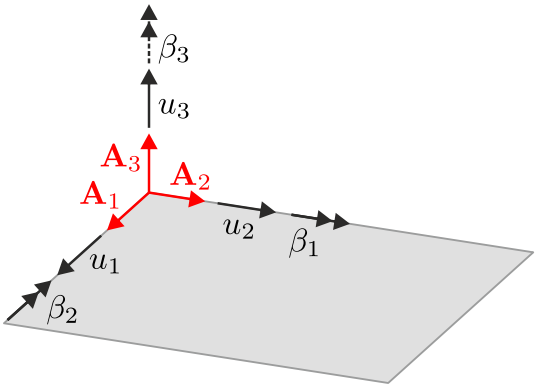

Fig. 2 Degrees of freedom of the shell related to the local Cartesian basis

2.2 Stress resultants and material law

In the framework of classical shell theory, all governing equations are mapped to the shell mid-surface. For the formulation of a material law, we define the work conjugate 2^{nd}-Piola-Kirchoff stress resultants and arrange them in the vector

$$\boldsymbol{\sigma} = \left[n^{11}, n^{22}, n^{12}, m^{11}, m^{22}, m^{12}, q^{13}, q^{23}\right]^T \ . \tag{11}$$

In general, they can be specified by integrating the 2^{nd}-Piola-Kirchoff stresses. Analogous to the shell strains, the shell stress resultants can be categorized into membrane forces

$$n^{\alpha\beta} = \int_{\zeta} S^{\alpha\beta} \mu \, \mathrm{d}\zeta \ , \tag{12}$$

bending moments

$$m^{\alpha\beta} = \int_{\zeta} \zeta \, S^{\alpha\beta} \mu \, \mathrm{d}\zeta \tag{13}$$

and shear forces

$$q^{\alpha 3} = \int_{\zeta} S^{\alpha 3} \mu \, \mathrm{d}\zeta \ . \tag{14}$$

For thin shells, the determinant of the shifter tensor is usually approximated by $\mu = 1$. All shell stress resultants are shown in Fig. 3.

A purely elastic material behavior is assumed for the shell. Due to the restriction to small strains, a linear relation between the 2^{nd}-Piola-Kirchhoff stresses and the Green-Lagrangian strains can be assumed. In order to describe the behavior of composite materials, a transversely isotropic layerwise formulation of the constitutive law is used. For a layer

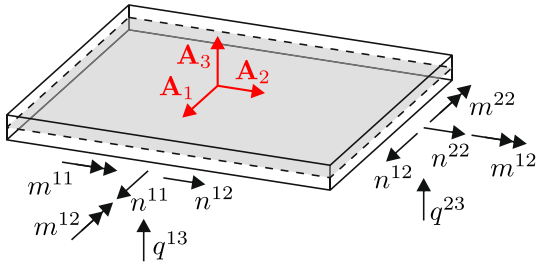

Fig. 3 Definition of the shell stress resultants

k, the local elasticity matrices are in general given by

$$\bar{\mathbf{C}}_m^k = \begin{bmatrix} C_{11} & C_{12} & 0 \\ C_{12} & C_{22} & 0 \\ 0 & 0 & C_{33} \end{bmatrix}, \qquad \bar{\mathbf{C}}_s^k = \begin{bmatrix} C_{44} & 0 \\ 0 & C_{55} \end{bmatrix}. \tag{15}$$

By applying a transformation, the global elasticity matrices $\mathbf{C}_m^k$ and $\mathbf{C}_s^k$ can be determined from the local properties in Eq. (15), see [35].With the summation over all layers, the following linear relationship between the nonlinear shell strains and stress resultants can be formulated

$$\boldsymbol{\sigma} = \mathbf{D}\,\boldsymbol{\varepsilon} \ , \quad \mathbf{D} = \begin{bmatrix} \mathbf{D}_m & \mathbf{D}_{mb} & \mathbf{0} \\ \mathbf{D}_{mb}^T & \mathbf{D}_b & \mathbf{0} \\ \mathbf{0} & \mathbf{0} & \mathbf{D}_s \end{bmatrix}. \tag{16}$$

The submatrices of the material matrix $\mathbf{D}$ are defined as

$$\begin{aligned} \mathbf{D}_m &= \sum_{k=1}^{nlay} \mathbf{C}_m^k \, h_k \ , \\ \mathbf{D}_b &= \sum_{k=1}^{nlay} \mathbf{C}_m^k \left(\frac{h_k^3}{12} + h_k \, \zeta_{sk}^2 \right) \ , \\ \mathbf{D}_{mb} &= \sum_{k=1}^{nlay} \mathbf{C}_m^k \, h_k \, \zeta_{sk} \ , \quad \mathbf{D}_s = \sum_{k=1}^{nlay} \mathbf{C}_s^k \, h_k \ . \end{aligned} \tag{17}$$

In Eq. (17), the total number of layers is $nlay$, the thickness of a single layer k is denoted by h_k and the distance from the center of the considered layer to the reference surface Ω_0 of the shell is given by ζ_{sk}.

2.3 Weak form-principle of virtual work

With the equations shown in the previous sections, the weak form defined on the shell mid-surface can be formulated

$$\begin{aligned} \delta\pi(\mathbf{v}, \delta\mathbf{v}) = \delta\pi_i - \delta\pi_{ext} &= \int_{\Omega_0} \delta\boldsymbol{\varepsilon}^T \boldsymbol{\sigma} \, \mathrm{d}A \\ &- \int_{\Omega_0} \delta\mathbf{v}^T \bar{\mathbf{q}} \, \mathrm{d}A - \int_{\partial\Omega_0^\sigma} \delta\mathbf{v}^T \bar{\mathbf{f}} \, \mathrm{d}s = 0 \, . \end{aligned} \tag{18}$$

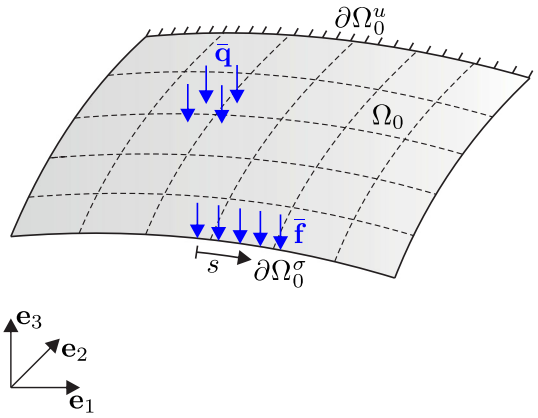

Fig. 4 Shell with boundary conditions in the reference configuration

It is given with respect to the undeformed shell configuration in a Total-Lagrangian description. The local displacement field of the shell is given by

$$\mathbf{v} = \left[u_1,\, u_2,\, u_3,\, \beta_1,\, \beta_2,\, \beta_3\right]^T \,. \tag{19}$$

The rotation β_3 around the local axis $\mathbf{A}_3$, see Fig. 2 is not included in the shell kinematics and can therefore be set to zero at the local level. Within the assembling procedure stiffness entries occur for all rotations at intersections of elements. Options for straight surfaces are discussed in detail in [36].

The first term in Eq. (18) describes the virtual work of the internal forces, while the last terms contain the virtual external work of surface tractions $\bar{\mathbf{q}}$ and edge loads $\bar{\mathbf{f}}$, see Fig. 4. In the following, we assume conservative loads.

To solve the nonlinear equation in Eq. (18) in the context of a Newton iteration scheme, the consistent linearization of the weak form is required. In general, this can be written as

$$\begin{aligned} \mathrm{L}\left[\delta\pi\right] &= \delta\pi + \Delta\delta\pi \\ &= \delta\pi + \int_{\Omega_0} \delta\boldsymbol{\varepsilon}^T \Delta\boldsymbol{\sigma}\, \mathrm{d}A + \int_{\Omega_0} \Delta\delta\boldsymbol{\varepsilon}^T \boldsymbol{\sigma}\, \mathrm{d}A = 0 \,. \end{aligned} \tag{20}$$

Within the finite element method, the linearized weak form (20) is discretized using a displacement field ansatz. All equations presented in this section form the basis for the spectral stochastic finite element formulation of the general shell element, described in Sect. 5.

3 Representation of stochastic quantities

We consider the probability space (Ω, Σ, P), where Ω is the event space, Σ the σ-algebra on Ω and P the probability measure on (Ω, Σ). A random variable X can be described by the mapping

$$X(\omega) : \Omega \mapsto D_X \subset \mathbb{R} \,. \tag{21}$$

Furthermore a set of M random variables is summarized in the random vector $\boldsymbol{X} = [X_1, \ldots, X_M]^T$. In this section, upper case letters are used for random variables and random vectors while realizations of these quantities are denoted by lower case letters. For the sake of simplicity, we assume that all components of $\boldsymbol{X}$ are stochastically independent. As a result, the joint probability density function (PDF) $f_{\boldsymbol{X}}(\boldsymbol{x})$ is the product of the M marginal distributions

$$f_{\boldsymbol{X}}(\boldsymbol{x}) = \prod_{i=1}^{M} f_{X_i}(x_i) \,. \tag{22}$$

Let $\mathscr{M}$ be a deterministic model that maps the M-dimensional input vector $\boldsymbol{x}$ to the scalar output variable z such that

$$\mathscr{M} : \boldsymbol{x} \in D_{\boldsymbol{X}} \subset \mathbb{R}^M \mapsto z \in D_Z \subset \mathbb{R} \,. \tag{23}$$

In the context of stochastic modeling, the input vector $\boldsymbol{x}$ is subjected by uncertainty, thus the output variable z is a random quantity

$$Z = \mathscr{M}(\boldsymbol{X}) \,. \tag{24}$$

3.1 Polynomial chaos expansion

Polynomial chaos expansion (PCE) is a widely used method for propagating parametric uncertainties through complex models. It was introduced in [3] for normally distributed random variables. In [5], the method has been extended to arbitrary probabilistic distributions of the model parameters. Assuming that the random variable Z in Eq. (24) has finite variance, an exact representation can be obtained with the PCE [37]

$$Z = \sum_{\alpha=0}^{\infty} z_\alpha \Psi_\alpha(\boldsymbol{X}) \,, \tag{25}$$

where z_α are deterministic coefficients and Ψ_α are orthonormal basis polynomials of the random input vector $\boldsymbol{X}$. The polynomials satisfy the orthonormality property

$$\begin{aligned} &\mathbb{E}\left[\Psi_\alpha(\boldsymbol{X})\, \Psi_\beta(\boldsymbol{X})\right] \\ &= \int_{D_{\boldsymbol{X}}} \Psi_\alpha(\boldsymbol{x})\, \Psi_\beta(\boldsymbol{x})\, f_{\boldsymbol{X}}(\boldsymbol{x})\, \mathrm{d}\boldsymbol{x} = \delta_{\alpha\beta} \end{aligned} \tag{26}$$

where $f_{\boldsymbol{X}}$ is the joint PDF of $\boldsymbol{X}$ and $\delta_{\alpha\beta}$ is the Kronecker delta. In order to achieve optimal convergence of the PCE, the polynomials used are chosen according to the probability

Table 1 Continuous distributions and associated polynomial basis, according to [4]

Type of distribution	Polynomial basis
Uniform	Legendre
Gaussian	Hermite
Gamma	Laguerre
Beta	Jacobi

density functions of the random input variables. Classical distributions and their corresponding polynomials are given in Table 1.

For a practical implementation, the infinite series in Eq. (25) has to be truncated to a finite sum of polynomials. This results in the following polynomial approximation of the random variable

$$\widehat{z} = \sum_{\alpha=0}^{P} z_\alpha \Psi_\alpha(\boldsymbol{X}) \approx Z \,. \tag{27}$$

Each polynomial Ψ_α is characterized by a so-called multi-index

$$\boldsymbol{m}_\alpha = [\, m_1, \,\ldots,\, m_i, \,\ldots,\, m_M \,], \quad m_i \in \mathbb{N} \,. \tag{28}$$

With the standard truncation criterion, only those polynomials are used, which have a total degree of $||\boldsymbol{m}||_1$ smaller than the specified maximum polynomial degree p, see [7]. The number of terms in the truncated polynomial chaos expansion (27) is given by

$$P = \frac{(M+p)!}{M!\,p!} - 1 \,. \tag{29}$$

Furthermore, we define $\bar{P} = P + 1$. All multi-indices $\boldsymbol{m}_\alpha$ with $\alpha \in [0, \ldots, P]$ can be summarized in the set

$$\mathscr{A}^{M,p} = \left\{ \boldsymbol{m} \in \mathbb{N}^M \,:\, ||\boldsymbol{m}||_1 \leq p \right\} \,. \tag{30}$$

For problems with many input variables, the so-called hyperbolic index set is proposed in [8], with

$$\begin{aligned} \mathscr{A}_q^{M,p} &= \left\{ \boldsymbol{m} \in \mathbb{N}^M \,:\, ||\boldsymbol{m}||_q \leq p \right\} \,, \\ ||\boldsymbol{m}||_q &= \left(\sum_{i=1}^{M} m_i^q \right)^{1/q} \,, \end{aligned} \tag{31}$$

where the parameter $q \in (0, 1]$ is used to control the truncation. In the following, this parameter q is referred to as q-norm. After choosing a set of polynomials $\mathscr{A}_q^{M,p}$ for the approximation, the unknown coefficients in Eq. (27) have to be determined. In Sect. 3.2, the mathematical operations for an intrusive calculation of the coefficients are shown.

3.2 Elementary operations with stochastic quantities

As part of the intrusive approach, the governing equations of the problem to be solved have to be modified. This requires various arithmetic operations of random variables, represented by the PCE. For a detailed description of the relations shown in this section and for the evaluation of non-polynomial functions, the reader is referred to [9].

In the following, random variables are characterized by their dependence on ω. Let $\widehat{b}$ and $\widehat{c}$ be known polynomial chaos expansions of the random variables $B(\omega)$ and $C(\omega)$ with

$$\widehat{b} = \sum_{\alpha=0}^{P} b_\alpha \Psi_\alpha \,, \qquad \widehat{c} = \sum_{\alpha=0}^{P} c_\alpha \Psi_\alpha \,. \tag{32}$$

In the following, representations given by Eq. (32) are referred to as PC variables or PC expansions. Appendix A contains a detailed description on how to represent normal and uniform distributed random variables in the context of the PCE. The PC variables (32) can be combined with each other using different arithmetic operations. This results in a new PC variable

$$\widehat{a} = \sum_{\alpha=0}^{P} a_\alpha \Psi_\alpha \,, \tag{33}$$

for which the coefficients a_α have to be determined.

Addition or subtraction operations

$$\widehat{a} = \widehat{b} \pm \widehat{c} \tag{34}$$

are calculated in the same way as in the deterministic case, i.e., the corresponding coefficients are just added or subtracted

$$a_\alpha = b_\alpha \pm c_\alpha \quad \forall \alpha \in \{0 \,\ldots, P\} \,. \tag{35}$$

The multiplication

$$\widehat{a} = \widehat{b} \cdot \widehat{c} \tag{36}$$

can be rewritten by inserting the existing PC expansions (32). This leads to

$$\widehat{a} = \sum_{\gamma=0}^{P} a_\gamma \Psi_\gamma$$

$$= \sum_{\alpha=0}^{P} b_\alpha \Psi_\alpha \sum_{\beta=0}^{P} c_\beta \Psi_\beta \; . \tag{37}$$

We assume that the result of the multiplication can be represented with the same polynomial basis as the PC variables themselves, even if the result has twice the polynomial order. The unknown coefficients of $\widehat{a}$ can be determined by means of a Galerkin projection leading to

$$\begin{aligned} a_\gamma &= \sum_{\alpha=0}^{P} \sum_{\beta=0}^{P} D_{\alpha\beta\gamma} \, b_\alpha \, c_\beta \\ &= D_{\alpha\beta\gamma} \, b_\alpha \, c_\beta \quad \forall \gamma \in \{0 \ldots, P\} \; , \end{aligned} \tag{38}$$

where the arising multiplication tensor $D_{\alpha\beta\gamma}$ is defined as

$$\begin{aligned} D_{\alpha\beta\gamma} &= \frac{\mathbb{E}\left[\Psi_\alpha \Psi_\beta \Psi_\gamma\right]}{\mathbb{E}\left[\Psi_\gamma \Psi_\gamma\right]} \\ &= \mathbb{E}\left[\Psi_\alpha \Psi_\beta \Psi_\gamma\right] \quad \alpha, \beta, \gamma \in [0, \ldots, P] \; . \end{aligned} \tag{39}$$

Since the basis polynomials satisfy the orthonormality property in Eq. (26), the denominator simplifies to $\mathbb{E}\left[\Psi_\gamma \Psi_\gamma\right] = \delta_{\gamma\gamma} = 1$. Analytical solutions for the expected values of the triple products of polynomials are shown in Appendix B. The calculation of a product of more than two PC variables can be reduced to the multiplication of two PC expansions by repeatedly using Eq. (38). This procedure is referred to as pseudospectral approach [9] and can be easily used for multiple multiplications. Appendix C illustrates the multiplication of two normal distributions.

Subsequently, the division

$$\widehat{a} = \widehat{c} \, / \, \widehat{b} \tag{40}$$

is solved by taking into account the relation in Eq. (38), i.e., the division operation of two polynomial chaos expansions leads to a set of equations for the unknown coefficients of $\widehat{a}$

$$D_{\alpha\beta\gamma} \, b_\alpha \, a_\beta = c_\gamma \quad \forall \gamma \in \{0 \ldots, P\} \; . \tag{41}$$

Compact notations of Eq. (38) and Eq. (41) are given in Appendix D.

3.3 Post-processing of PC variables

In the context of a stochastic analysis, the use of PC expansions provides some advantages. Due to the orthonormality property of the polynomials (26), statistical moments such as mean value and variance can be determined from an existing PC expansion (27)

$$\mu_{\widehat{z}} = z_0$$

$$\sigma^2_{\widehat{z}} = \sum_{\alpha=1}^{P} z_\alpha^2 \; . \tag{42}$$

The multiplication tensor (39) can also be used to calculate higher stochastic moments such as the skewness

$$\begin{aligned} \delta_{\widehat{z}} &= \frac{1}{\sigma^3_{\widehat{z}}} \sum_{\alpha=1}^{P} \sum_{\beta=1}^{P} \sum_{\gamma=1}^{P} \mathbb{E}\left[\Psi_\alpha \Psi_\beta \Psi_\gamma\right] z_\alpha \, z_\beta \, z_\gamma \\ &= \frac{1}{\sigma^3_{\widehat{z}}} \sum_{\alpha=1}^{P} \sum_{\beta=1}^{P} \sum_{\gamma=1}^{P} D_{\alpha\beta\gamma} \, z_\alpha \, z_\beta \, z_\gamma \; . \end{aligned} \tag{43}$$

Furthermore, variance-based sensitivity measures, such as Sobol' indices [38], can be derived from the PC coefficients. For a detailed description and computation of the so-called PCE-based Sobol' indices, the reader is referred to [39].

4 Stochastic variational formulation for geometric nonlinear shells

The stochastic version of the weak form in Eq. (18) for the shell formulation presented in Sect. 2 is given by

$$\begin{aligned} &\mathbb{E}\left[\delta\pi(\omega)\right] = \mathbb{E}\left[\delta\pi_i(\omega) - \delta\pi_{ext}(\omega)\right] \\ &= \mathbb{E}\left[\int_{\Omega_0} \delta\boldsymbol{\varepsilon}^T(\omega)\boldsymbol{\sigma}(\omega) \, \mathrm{d}A - \delta\pi_{ext}(\omega)\right] = 0 \; . \end{aligned} \tag{44}$$

In the following, all stochastic quantities are characterized by their dependence on ω. To solve the nonlinear equation in Eq. (44) in the context of a Newton iteration scheme, the consistent linearization is required, which results in

$$\begin{aligned} &\mathrm{L}\left[\mathbb{E}\left[\delta\pi(\omega)\right]\right] = \mathbb{E}\left[\delta\pi(\omega) + \Delta\delta\pi(\omega)\right] \\ &= \mathbb{E}\left[\delta\pi(\omega) + \int_{\Omega_0} \delta\boldsymbol{\varepsilon}^T(\omega)\Delta\boldsymbol{\sigma}(\omega) + \Delta\delta\boldsymbol{\varepsilon}^T(\omega)\boldsymbol{\sigma}(\omega) \, \mathrm{d}A\right] \\ &= 0 \; . \end{aligned} \tag{45}$$

To determine the variation and linearization of the stochastic variables in Eq. (45), these quantities are represented by the PCE. This stochastic discretization is described in the following section.

4.1 PC expansion of stochastic quantities

Due to the stochastic modeling of various material and geometrical parameters, the displacement field of the shell is a

random quantity, denoted by $\mathbf{v}(\omega)$. As described in Sect. 3.1, the corresponding PC expansion $\widehat{\mathbf{v}}$ can be formulated as

$$\mathbf{v}(\omega) \approx \widehat{\mathbf{v}} = \sum_{\alpha=0}^{P} \mathbf{v}_\alpha \Psi_\alpha = \sum_{\alpha} \mathbf{v}_\alpha \Psi_\alpha \ . \tag{46}$$

with the coefficients arranged in the vector

$$\mathbf{v} = \left[\mathbf{v}_0^T \ldots \mathbf{v}_\alpha^T \ldots \mathbf{v}_P^T\right]^T, \quad \mathbf{v} \in \mathbb{R}^{6\bar{P}} \ . \tag{47}$$

One particular coefficient of the displacement vector contains the corresponding displacement values

$$\mathbf{v}_\alpha = \left[u_{1\alpha},\, u_{2\alpha},\, u_{3\alpha},\, \beta_{1\alpha},\, \beta_{2\alpha},\, 0\right]^T \ . \tag{48}$$

The nonlinear shell strains depending on the stochastic displacements are completely described by their PC coefficients and can be represented by

$$\boldsymbol{\varepsilon}(\omega) \approx \widehat{\boldsymbol{\varepsilon}} = \sum_{\gamma} \boldsymbol{\varepsilon}_\gamma \, \Psi_\gamma \ . \tag{49}$$

Stochastic arithmetic operations, introduced in Sect. 3.2, are required to determine the corresponding coefficients. They can be summarized in the vector

$$\boldsymbol{\varepsilon}_\gamma = \begin{bmatrix} u_{1\gamma,1} + \frac{1}{2} D_{\alpha\beta\gamma} (u_{1\alpha,1}\, u_{1\beta,1} \\ +u_{2\alpha,1}\, u_{2\beta,1} + u_{3\alpha,1}\, u_{3\beta,1}) \\ u_{2\gamma,2} + \frac{1}{2} D_{\alpha\beta\gamma} (u_{1\alpha,2}\, u_{1\beta,2} \\ +u_{2\alpha,2}\, u_{2\beta,2} + u_{3\alpha,2}\, u_{3\beta,2}) \\ u_{1\gamma,2} + u_{2\gamma,1} + D_{\alpha\beta\gamma} (u_{1\alpha,1}\, u_{1\beta,2} \\ +u_{2\alpha,1}\, u_{2\beta,2} + u_{3\alpha,1}\, u_{3\beta,2}) \\ \beta_{1\gamma,1} \\ \beta_{2\gamma,2} \\ \beta_{1\gamma,2} + \beta_{2\gamma,1} \\ \beta_{1\gamma} + u_{3\gamma,1} \\ \beta_{2\gamma} + u_{3\gamma,2} \end{bmatrix} . \tag{50}$$

For the sake of simplicity, the summation signs are dropped. According to the Einstein convention, the summation is carried out over the indices that appear twice. For a compact representation, all coefficients can be arranged in $\boldsymbol{\varepsilon} \in \mathbb{R}^{8\bar{P}}$

$$\boldsymbol{\varepsilon} = \begin{bmatrix} \boldsymbol{\varepsilon}_0 \\ \vdots \\ \boldsymbol{\varepsilon}_\gamma \\ \vdots \\ \boldsymbol{\varepsilon}_P \end{bmatrix}, \qquad \boldsymbol{\varepsilon}_\gamma = \begin{bmatrix} \varepsilon_{11\gamma} \\ \varepsilon_{22\gamma} \\ 2\varepsilon_{12\gamma} \\ \kappa_{11\gamma} \\ \kappa_{22\gamma} \\ 2\kappa_{12\gamma} \\ \gamma_{13\gamma} \\ \gamma_{23\gamma} \end{bmatrix} . \tag{51}$$

Based on the definition in Eq. (50), the variation and linearization of the stochastic shell strains can be calculated.

We assume that structural parameters, e.g. the Young's modulus, are subjected by uncertainty, thus the material matrix (16) of the shell is a stochastic matrix. It can be represented by its deterministic coefficients using the PCE. In general, the associated PC expansion is given by

$$\mathbf{D}(\omega) \approx \widehat{\mathbf{D}} = \sum_{\alpha} \mathbf{D}_\alpha \Psi_\alpha \ . \tag{52}$$

To determine the unknown coefficients $\mathbf{D}_\alpha$, the stochastic structural parameter, e.g. the Young's modulus of the shell, is first represented by a PCE. This PC expansion can subsequently be used to compute the coefficients of the material matrix. For this purpose, the arithmetic operations, proposed in Sect. 3.2, are required. This uncertainty propagation is shown in Appendix E by means of an example.

Since we assume a linear elastic material law, the coefficients of the shell stress resultants can be calculated with the stochastic multiplication as follows

$$\begin{aligned} \boldsymbol{\sigma}_\gamma &= D_{\alpha\beta\gamma}\, \mathbf{D}_\alpha\, \boldsymbol{\varepsilon}_\beta \\ &= \mathbf{D}_{\gamma\beta}\, \boldsymbol{\varepsilon}_\beta \ . \end{aligned} \tag{53}$$

Due to the symmetries of the multiplication tensor (127), the relation $\mathbf{D}_{\gamma\beta} = \mathbf{D}_{\beta\gamma}$ holds. The submatrices $\mathbf{D}_{\gamma\beta}$ defined in Eq. (53) can be arranged in the augmented material matrix $\mathbf{D} \in \mathbb{R}^{8\bar{P}\times 8\bar{P}}$ defined as

$$\mathbf{D} = \begin{bmatrix} \mathbf{D}_{00} & \cdots & \mathbf{D}_{0\beta} & \cdots & \mathbf{D}_{0P} \\ \vdots & \ddots & \vdots & \ddots & \vdots \\ \mathbf{D}_{\gamma 0} & \cdots & \mathbf{D}_{\gamma\beta} & \cdots & \mathbf{D}_{\gamma P} \\ \vdots & \ddots & \vdots & \ddots & \vdots \\ \mathbf{D}_{P0} & \cdots & \mathbf{D}_{P\beta} & \cdots & \mathbf{D}_{PP} \end{bmatrix} . \tag{54}$$

The coefficients of the stress resultants are merged analogous to the shell strains in the vector $\boldsymbol{\sigma} \in \mathbb{R}^{8\bar{P}}$ with

$$\boldsymbol{\sigma} = \begin{bmatrix} \boldsymbol{\sigma}_0 \\ \vdots \\ \boldsymbol{\sigma}_\gamma \\ \vdots \\ \boldsymbol{\sigma}_P \end{bmatrix}, \qquad \boldsymbol{\sigma}_\gamma = \begin{bmatrix} n_\gamma^{11} \\ n_\gamma^{22} \\ n_\gamma^{12} \\ m_\gamma^{11} \\ m_\gamma^{22} \\ m_\gamma^{12} \\ q_\gamma^{13} \\ q_\gamma^{23} \end{bmatrix} . \tag{55}$$

With the variables defined above, the linear-elastic material law can be formulated compactly as

$$\boldsymbol{\sigma} = \mathbf{D}\, \boldsymbol{\varepsilon} \ . \tag{56}$$

4.2 Variation of stochastic shell strains

Based on the polynomial chaos expansion of the shell strains (51), the variation and linearization of these quantities can be derived. Therefore, we form the directional derivative of the shell strains PC coefficients (50) with respect to the PC coefficients of the desired displacement quantities. For the sake of simplicity, all derivations below are shown for one individual coefficient of the stochastic quantity. Thus, the variation of the membrane strain coefficient $\varepsilon_{11\gamma}$ is given by

$$\begin{aligned}\delta\varepsilon_{11\gamma} &= \frac{\partial\varepsilon_{11\gamma}}{\partial u_{1\lambda,1}}\delta u_{1\lambda,1} + \frac{\partial\varepsilon_{11\gamma}}{\partial u_{2\lambda,1}}\delta u_{2\lambda,1} + \frac{\partial\varepsilon_{11\gamma}}{\partial u_{3\lambda,1}}\delta u_{3\lambda,1} \\ &= \delta_{\gamma\lambda}\delta u_{1\lambda,1} + \frac{1}{2}D_{\alpha\beta\gamma}\left(\delta_{\alpha\lambda}u_{1\beta,1} + \delta_{\beta\lambda}u_{1\alpha,1}\right)\delta u_{1\lambda,1} \\ &\quad + \frac{1}{2}D_{\alpha\beta\gamma}\left(\delta_{\alpha\lambda}u_{2\beta,1} + \delta_{\beta\lambda}u_{2\alpha,1}\right)\delta u_{2\lambda,1} \\ &\quad + \frac{1}{2}D_{\alpha\beta\gamma}\left(\delta_{\alpha\lambda}u_{3\beta,1} + \delta_{\beta\lambda}u_{3\alpha,1}\right)\delta u_{3\lambda,1}\,. \end{aligned} \tag{57}$$

Taking into account the symmetry properties of the multiplication tensor, Eq. (57) can be simplified to

$$\begin{aligned}\delta\varepsilon_{11\gamma} &= (\delta_{\lambda\gamma} + D_{\alpha\beta\gamma}\delta_{\alpha\lambda}u_{1\beta,1})\delta u_{1\lambda,1} \\ &\quad + (D_{\alpha\beta\gamma}\delta_{\alpha\lambda}u_{2\beta,1})\delta u_{2\lambda,1} + (D_{\alpha\beta\gamma}\delta_{\alpha\lambda}u_{3\beta,1})\delta u_{3\lambda,1}\,. \end{aligned} \tag{58}$$

The variation of a quantity is indicated by the letter $\delta(\bullet)$ while $\delta_{\lambda\mu}$ are Kronecker deltas resulting from the partial derivative. Taking into account the relationship (128), the variation can be finally rewritten as

$$\begin{aligned}\delta\varepsilon_{11\gamma} &= D_{\lambda\beta\gamma}\left[(\delta_{\beta0} + u_{1\beta,1})\delta u_{1\lambda,1} + u_{2\beta,1}\delta u_{2\lambda,1}\right. \\ &\quad \left. + u_{3\beta,1}\delta u_{3\lambda,1}\right]. \end{aligned} \tag{59}$$

A detailed derivation of the remaining variations can be found in Appendix F. All results can thus be arranged in the vector

$$\delta\boldsymbol{\varepsilon}_\gamma = D_{\lambda\beta\gamma}\begin{bmatrix} (\delta_{\beta0} + u_{1\beta,1})\delta u_{1\lambda,1} + u_{2\beta,1}\delta u_{2\lambda,1} \\ +u_{3\beta,1}\delta u_{3\lambda,1} \\ u_{1,2\beta}\delta u_{1\lambda,2} + (\delta_{\beta0} + u_{2\beta,2})\delta u_{2\lambda,2} \\ +u_{3\beta,2}\delta u_{3\lambda,2} \\ u_{1,2\beta}\delta u_{1\lambda,1} + (\delta_{\beta0} + u_{1\beta,1})\delta u_{1\lambda,2} \\ +(\delta_{\beta0} + u_{2\beta,2})\delta u_{2\lambda,1} + u_{2\beta,1}\delta u_{2\lambda,2} \\ +u_{3\beta,2}\delta u_{3\lambda,1} + u_{3\beta,1}\delta u_{3\lambda,2} \\ \delta_{\beta0}\delta\beta_{1\lambda,1} \\ \delta_{\beta0}\delta\beta_{2\lambda,2} \\ \delta_{\beta0}\delta\beta_{1\lambda,2} + \delta_{\beta0}\delta\beta_{2\lambda,1} \\ \delta_{\beta0}\delta\beta_{1\lambda} + \delta_{\beta0}\delta u_{3\lambda,1} \\ \delta_{\beta0}\delta\beta_{2\lambda} + \delta_{\beta0}\delta u_{3\lambda,2} \end{bmatrix} \tag{60}$$

and the PC expansion of the virtual stochastic shell strains reads

$$\delta\widehat{\boldsymbol{\varepsilon}} = \sum_\gamma \delta\boldsymbol{\varepsilon}_\gamma\,\Psi_\gamma \approx \delta\boldsymbol{\varepsilon}(\omega)\,. \tag{61}$$

All associated coefficients are arranged in

$$\delta\boldsymbol{\varepsilon} = \left[\delta\boldsymbol{\varepsilon}_0^T \ldots \delta\boldsymbol{\varepsilon}_\gamma^T \ldots \delta\boldsymbol{\varepsilon}_P^T\right]^T\,. \tag{62}$$

4.3 Linearization of the material law

Within the linearized stochastic virtual work (45), the linearization of the stochastic stress resultants is needed. Taking into account Eq. (53), the linearization of this stochastic variables can be written as

$$\begin{aligned}\Delta\boldsymbol{\sigma}_\gamma &= \frac{\partial\boldsymbol{\sigma}_\gamma}{\partial\boldsymbol{\varepsilon}_\mu}\Delta\boldsymbol{\varepsilon}_\mu = \frac{\partial\left(D_{\alpha\beta\gamma}\,\mathbf{D}_\alpha\boldsymbol{\varepsilon}_\beta\right)}{\partial\boldsymbol{\varepsilon}_\mu}\Delta\boldsymbol{\varepsilon}_\mu \\ &= D_{\alpha\beta\gamma}\,\delta_{\beta\mu}\mathbf{D}_\alpha\Delta\boldsymbol{\varepsilon}_\mu = D_{\alpha\mu\gamma}\,\mathbf{D}_\alpha\Delta\boldsymbol{\varepsilon}_\mu \\ &= \mathbf{D}_{\gamma\mu}\,\Delta\boldsymbol{\varepsilon}_\mu\,. \end{aligned} \tag{63}$$

The coefficients of the linearized shell strains are determined analogously to its variation (60) by replacing $\delta(\bullet)$ with $\Delta(\bullet)$. Finally, this results in the chaos expansion

$$\Delta\widehat{\boldsymbol{\varepsilon}} = \sum_\mu \Delta\boldsymbol{\varepsilon}_\mu\,\Psi_\mu \approx \Delta\boldsymbol{\varepsilon}(\omega)\,. \tag{64}$$

4.4 Linearization of virtual shell strains

In the context of geometrical nonlinear formulations, the additional term $\Delta\delta\boldsymbol{\varepsilon}(\omega)$ occurs during the linearization of the weak form. The corresponding coefficients can be calculated in a similar way as shown in the previous sections. The linearization of the virtual membrane strain coefficient $\delta\varepsilon_{11\gamma}$ can be written as

$$\begin{aligned}\Delta\delta\varepsilon_{11\gamma} &= \frac{\partial\delta\varepsilon_{11\gamma}}{\partial u_{1\mu,1}}\Delta u_{1\mu,1} + \frac{\partial\delta\varepsilon_{11\gamma}}{\partial u_{2\mu,1}}\Delta u_{2\mu,1} + \frac{\partial\delta\varepsilon_{11\gamma}}{\partial u_{3\mu,1}}\Delta u_{3\mu,1} \\ &= D_{\lambda\beta\gamma}\delta_{\beta\mu}\left[\delta u_{1\lambda,1}\Delta u_{1\mu,1} + \delta u_{2\lambda,1}\Delta u_{2\mu,1}\right. \\ &\quad \left. + \delta u_{3\lambda,1}\Delta u_{3\mu,1}\right] \\ &= D_{\lambda\mu\gamma}\left[\delta u_{1\lambda,1}\Delta u_{1\mu,1} + \delta u_{2\lambda,1}\Delta u_{2\mu,1}\right. \\ &\quad \left. + \delta u_{3\lambda,1}\Delta u_{3\mu,1}\right]\,. \end{aligned} \tag{65}$$

A detailed derivation of the remaining quantities can be found in Appendix G. The restriction to moderate rotations results in non-zero components of the membrane strains only.

Finally, the coefficients

$$\Delta\delta\boldsymbol{\varepsilon}_\gamma = D_{\lambda\mu\gamma} \begin{bmatrix} \delta u_{1\lambda,1}\,\Delta u_{1\mu,1} + \delta u_{2\lambda,1}\,\Delta u_{2\mu,1} \\ +\delta u_{3\lambda,1}\,\Delta u_{3\mu,1} \\ \delta u_{1\lambda,2}\,\Delta u_{1\mu,2} + \delta u_{2\lambda,2}\,\Delta u_{2\mu,2} \\ +\delta u_{3\lambda,2}\,\Delta u_{3\mu,2} \\ \delta u_{1\lambda,2}\,\Delta u_{1\mu,1} + \delta u_{1\lambda,1}\,\Delta u_{1\mu,2} \\ +\delta u_{2\lambda,2}\,\Delta u_{2\mu,1} + \delta u_{2\lambda,1}\,\Delta u_{2\mu,2} \\ +\delta u_{3\lambda,2}\,\Delta u_{3\mu,1} + \delta u_{3\lambda,1}\,\Delta u_{3\mu,2} \\ 0 \\ 0 \\ 0 \\ 0 \\ 0 \end{bmatrix} \tag{66}$$

are used to define the PC expansion of the linearized virtual shell strains

$$\Delta\delta\widehat{\boldsymbol{\varepsilon}} = \sum_\gamma \Delta\delta\boldsymbol{\varepsilon}_\gamma\,\Psi_\gamma \approx \Delta\delta\boldsymbol{\varepsilon}(\omega)\,. \tag{67}$$

4.5 Stochastic discretization of the weak form

The linearized stochastic weak form (45) can now be discretized with the derived chaos expansions and thus transformed into deterministic equations. For the discretized virtual work of the internal and external forces, we obtain

$$\begin{aligned}&\mathbb{E}\left[\delta\pi(\omega)\right] \\ &= \int_{\Omega_0} \delta\boldsymbol{\varepsilon}_\alpha^T\,\boldsymbol{\sigma}_\alpha\,\mathrm{d}A - \int_{\Omega_0} \delta\mathbf{v}_\alpha^T\,\bar{\mathbf{q}}_\alpha\,\mathrm{d}A - \int_{\partial\Omega_0^\sigma} \delta\mathbf{v}_\alpha^T\,\bar{\mathbf{f}}_\alpha\,\mathrm{d}s\,.\end{aligned} \tag{68}$$

The linearization can be written as

$$\begin{aligned}&\mathrm{L}\left[\mathbb{E}\left[\delta\pi(\omega)\right]\right] \\ &= \mathbb{E}\left[\delta\pi(\omega)\right] + \int_{\Omega_0} \delta\boldsymbol{\varepsilon}_\alpha^T\,\mathbf{D}_\beta\,\Delta\boldsymbol{\varepsilon}_\gamma\,D_{\alpha\beta\gamma} + \Delta\delta\boldsymbol{\varepsilon}_\alpha^T\,\boldsymbol{\sigma}_\alpha\,\mathrm{d}A\,.\end{aligned} \tag{69}$$

For a detailed derivation of the relations shown here, the reader is referred to Appendix H. At this point, it should be noted that Eq. (68) and (69) are discrete in the stochastic dimension but still continuous in the displacement quantities sought. A discretization of these field variables is carried out in the context of the finite element method.

4.6 Consistency of the stochastic variational formulation

The stochastic variational formulation presented in the previous sections are an extension of the deterministic equations. This connection will be illustrated and discussed below. When no randomness is considered in the problem, all stochastic quantities reduce to deterministic ones. Deterministic variables, e.g. the displacement u_1, can be represented by a PC expansion with

$$u_1 = \sum_\alpha u_{1\alpha}\Psi_\alpha\,, \quad u_{1\alpha} = 0 \quad \forall\alpha > 0\,. \tag{70}$$

Since deterministic quantities have no variance, only the first coefficient is non-zero. The coefficients $u_{1\alpha}$ are given by

$$u_{1\alpha} = u_{10}\delta_{\alpha 0}\,. \tag{71}$$

At this point, it should be noted again that $\delta_{\alpha 0}$ is the Kronecker delta. The coefficient $\varepsilon_{11\gamma}$ of the membrane strain can therefore be written as

$$\begin{aligned}\varepsilon_{11\gamma} &= u_{10,1}\delta_{\gamma 0} + \frac{1}{2}D_{\alpha\beta\gamma}(u_{10,1}\delta_{\alpha 0}u_{10,1}\delta_{\beta 0} \\ &\quad + u_{20,1}\delta_{\alpha 0}u_{20,1}\delta_{\beta 0} + u_{30,1}\delta_{\alpha 0}u_{30,1}\delta_{\beta 0}) \\ &= u_{10,1}\delta_{\gamma 0} + \frac{1}{2}D_{00\gamma}(u_{10,1}\,u_{10,1} \\ &\quad + u_{20,1}\,u_{20,1} + u_{30,1}\,u_{30,1}) \\ &= \delta_{\gamma 0}\left(u_{10,1} + \frac{1}{2}(u_{10,1}^2 + u_{20,1}^2 + u_{30,1}^2)\right)\,.\end{aligned} \tag{72}$$

In comparison to Eq. (50), Eq. (72) shows that only the first coefficient with $\gamma = 0$ is not equal to zero. Furthermore, it can be seen that the stochastic multiplication with $D_{\alpha\beta\gamma}$ is reduced to a deterministic multiplication. Equation (72) therefore just matches the first line of Eq. (10). In the deterministic case, the coefficients of the shell strains (51) simplify to

$$\boldsymbol{\varepsilon} = \begin{bmatrix} \delta_{00}\boldsymbol{\varepsilon}_0 \\ \vdots \\ \delta_{\gamma 0}\boldsymbol{\varepsilon}_0 \\ \vdots \\ \delta_{P0}\boldsymbol{\varepsilon}_0 \end{bmatrix} = \begin{bmatrix} \boldsymbol{\varepsilon}_0 \\ \vdots \\ \mathbf{0} \\ \vdots \\ \mathbf{0} \end{bmatrix}\,. \tag{73}$$

The augmented material matrix can be reduced to

$$\mathbf{D} = D_{\alpha\beta\gamma}\mathbf{D}_0\delta_{\alpha 0} = \delta_{\beta\gamma}\mathbf{D}_0 = \begin{bmatrix} \mathbf{D}_0 & \cdots & \mathbf{0} & \cdots & \mathbf{0} \\ \vdots & \ddots & \vdots & \ddots & \vdots \\ \mathbf{0} & \cdots & \mathbf{D}_0 & \cdots & \mathbf{0} \\ \vdots & \ddots & \vdots & \ddots & \vdots \\ \mathbf{0} & \cdots & \mathbf{0} & \cdots & \mathbf{D}_0 \end{bmatrix} . \quad (74)$$

The properties shown in Eqs. (73) and (74) can be transferred to other variables in a similar way.

5 Spectral stochastic FE-formulation for geometric nonlinear shells

In this section, the spectral stochastic finite element formulation for a shell based on the isoparametric concept is presented. For a general finite element discretization

$$\Omega_0 \approx \Omega^h = \bigcup_{e=1}^{n_e} \Omega^e , \quad (75)$$

the shell mid-surface Ω_0 is discretized with n_e elements. A local Cartesian coordinate system $\mathbf{A}_i$ is introduced at the center of each element e. The transformation matrix $\mathbf{T}$, defined in Appendix I, links the global coordinate system $\mathbf{e}_i$ with the local basis $\mathbf{A}_i$.

5.1 Mid-surface and displacement interpolation

Within a single element Ω^e, the geometry and displacements are interpolated with bi-linear functions

$$N_I = \frac{1}{4}(1+\xi_I\xi)(1+\eta_I\eta) ,$$
$$\xi_I \in \{-1, 1, 1, -1\} , \quad \eta_I \in \{-1, -1, 1, 1\} \quad (76)$$

defined in the unit element $\{\xi, \eta\} \in [-1, 1]$.

The reference configuration is deterministic, so that the position vector can be approximated with

$$\mathbf{X} \approx \mathbf{X}^h = \sum_{I=1}^{4} N_I \mathbf{X}_I . \quad (77)$$

Since we assume that structural parameters of the shell are subject to uncertainties, the displacements are stochastic quantities. The displacement ansatz is given by

$$\mathbf{v}(\omega) = \sum_{\alpha} \sum_{I=1}^{4} N_I \, \mathbf{v}_{I\alpha} \, \Psi_\alpha \quad (78)$$

using the bi-linear shape functions N_I for the spatial interpolation and the orthonormal polynomials Ψ_α for the stochastic approximation. The virtual and linearized displacements are interpolated in the same way. The corresponding coefficients of the nodal displacement vector are given by

$$\mathbf{v}_{I\alpha} = \left[u_{1I\alpha}, \, u_{2I\alpha}, \, u_{3I\alpha}, \, \beta_{1I\alpha}, \, \beta_{2I\alpha}, \, 0\right]^T = \left[\mathbf{u}_{I\alpha}, \, \boldsymbol{\beta}_{I\alpha}\right]^T . \quad (79)$$

In a five-parameter shell kinematics, the local sixth degree of freedom is set to zero. Considering a single chaos coefficient, the approximation follows from Eq. (78)

$$\mathbf{v}_\alpha = \sum_{I=1}^{4} N_I \, \mathbf{v}_{I\alpha} = \sum_{I} N_I \, \mathbf{v}_{I\alpha} . \quad (80)$$

For the sake of clarity, the following equations are usually presented for a specific PC coefficient of the corresponding quantity. In order to calculate the nonlinear shell strains, it is necessary to determine the derivatives of the displacements with respect to the local Cartesian base system $\mathbf{A}_j$, which can be formulated as

$$\mathbf{v}_{\alpha,j} = \sum_{I} N_{I,j} \, \mathbf{v}_{I\alpha} , \quad j = 1, 2 . \quad (81)$$

For this purpose, the Jacobian matrix is defined as

$$\mathbf{J} = \frac{\partial \mathbf{X}}{\partial \boldsymbol{\xi}} = \sum_{I=1}^{4} \mathbf{X}_I \otimes \nabla_{\boldsymbol{\xi}} N_I . \quad (82)$$

Its inverse is used to determine the local Cartesian derivatives of the shape functions

$$\begin{bmatrix} N_{I,1} \\ N_{I,2} \end{bmatrix} = \mathbf{J}^{-T} \begin{bmatrix} N_{I,\xi} \\ N_{I,\eta} \end{bmatrix} . \quad (83)$$

5.2 Interpolation of virtual and linearized shell strains

Within the weak form, the deterministic coefficients of the virtual shell strains, defined in (60) have to be approximated. In general, the finite element interpolation can be written with the so-called $\mathbf{B}$-matrices

$$\delta\boldsymbol{\varepsilon}_\gamma = \sum_{I} \underbrace{D_{\lambda\beta\gamma} \begin{bmatrix} \mathbf{B}^m_{I\beta} & \mathbf{0}_{3\times 2} & 0 \\ \mathbf{0}_{3\times 3} & \mathbf{B}^b_{I\beta} & 0 \\ \mathbf{0}_{2\times 2} & \mathbf{B}^s_{I\beta} & 0 \end{bmatrix}}_{\mathbf{B}_{I\lambda\gamma}} \delta\mathbf{v}_{I\lambda} . \quad (84)$$

The sub-matrix $\mathbf{B}^m_{I\beta}$ for the approximation of the membrane strains can be divided into a linear (l) and a nonlinear (nl)

part

$$\mathbf{B}^{m}_{I\beta} = \mathbf{B}^{m,l}_{I\beta} + \mathbf{B}^{m,nl}_{I\beta} \ , \tag{85}$$

with

$$\mathbf{B}^{m,l}_{I\beta} = \begin{bmatrix} \delta_{\beta 0}\, N_{I,1} & 0 & 0 \\ 0 & \delta_{\beta 0}\, N_{I,2} & 0 \\ \delta_{\beta 0}\, N_{I,2} & \delta_{\beta 0}\, N_{I,1} & 0 \end{bmatrix} ,$$

$$\mathbf{B}^{m,nl}_{I\beta} = \begin{bmatrix} u_{1\beta,1} N_{I,1} & u_{2\beta,1} N_{I,1} & u_{3\beta,1} N_{I,1} \\ u_{1\beta,2} N_{I,2} & u_{2\beta,2} N_{I,2} & u_{3\beta,2} N_{I,2} \\ u_{1\beta,1} N_{I,2} & u_{2\beta,1} N_{I,2} & u_{3\beta,1} N_{I,2} \\ +u_{1\beta,2} N_{I,1} & +u_{2\beta,2} N_{I,1} & +u_{3\beta,2} N_{I,1} \end{bmatrix} . \tag{86}$$

Furthermore, the matrices $\mathbf{B}^{b}_{I\beta}$ and $\mathbf{B}^{s}_{I\beta}$ can be specified as

$$\mathbf{B}^{b}_{I\beta} = \begin{bmatrix} 0 & \delta_{\beta 0}\, N_{I,1} \\ -\delta_{\beta 0}\, N_{I,2} & 0 \\ -\delta_{\beta 0}\, N_{I,1} & -\delta_{\beta 0}\, N_{I,2} \end{bmatrix} \tag{87}$$

and

$$\mathbf{B}^{s}_{I\beta} = \begin{bmatrix} \delta_{\beta 0}\, N_{I,1} & 0 & \delta_{\beta 0}\, N_{I} \\ \delta_{\beta 0}\, N_{I,2} & -\delta_{\beta 0}\, N_{I} & 0 \end{bmatrix} . \tag{88}$$

The restriction to moderate rotations means that the curvatures and shear strains are still linear in the displacements. This property can be seen from Eqs. (87) and (88), as each entry of the matrices contains the Kronecker delta $\delta_{\beta 0}$. Finally, the finite element approximation of the virtual shell strains can be written as

$$\delta\boldsymbol{\varepsilon}_{\gamma} = \sum_{I} \mathbf{B}_{I\gamma\lambda}\, \delta\mathbf{v}_{I\lambda}$$

$$\begin{bmatrix} \delta\boldsymbol{\varepsilon}_0 \\ \vdots \\ \delta\boldsymbol{\varepsilon}_{\gamma} \\ \vdots \\ \delta\boldsymbol{\varepsilon}_{P} \end{bmatrix} = \sum_{I} \begin{bmatrix} \mathbf{B}_{I00} & \cdots & \mathbf{B}_{I0\lambda} & \cdots & \mathbf{B}_{I0P} \\ \vdots & \ddots & \vdots & \ddots & \vdots \\ \mathbf{B}_{I\gamma 0} & \cdots & \mathbf{B}_{I\gamma\lambda} & \cdots & \mathbf{B}_{I\gamma P} \\ \vdots & \ddots & \vdots & \ddots & \vdots \\ \mathbf{B}_{IP0} & \cdots & \mathbf{B}_{IP\lambda} & \cdots & \mathbf{B}_{IPP} \end{bmatrix} \begin{bmatrix} \delta\mathbf{v}_{I0} \\ \vdots \\ \delta\mathbf{v}_{I\lambda} \\ \vdots \\ \delta\mathbf{v}_{IP} \end{bmatrix} . \tag{89}$$

With the introduction of the augmented **B**-matrix, the variation of the nonlinear shell strains can be written compactly in a common notation

$$\delta\boldsymbol{\varepsilon} = \sum_{I} \mathbf{B}_{I}\, \delta\mathbf{v}_{I} \ . \tag{90}$$

The approximation of the linearized shell strains $\Delta\boldsymbol{\varepsilon}$ can be written in the same way as in Eq. (90)

$$\Delta\boldsymbol{\varepsilon} = \sum_{K} \mathbf{B}_{K}\, \Delta\mathbf{v}_{K} \ . \tag{91}$$

5.3 Interpolation of linearized virtual shell strains

Since nonlinear components only occur in the membrane strains, the product $\Delta\delta\boldsymbol{\varepsilon}^{T}_{\alpha}\boldsymbol{\sigma}_{\alpha}$ in Eq. (69) simplifies to

$$\Delta\delta\boldsymbol{\varepsilon}^{T}_{\alpha}\boldsymbol{\sigma}_{\alpha} = \Delta\delta\varepsilon_{11\alpha}\, n^{11}_{\alpha} + 2\Delta\delta\varepsilon_{12\alpha}\, n^{12}_{\alpha} + \Delta\delta\varepsilon_{22\alpha}\, n^{22}_{\alpha} \ . \tag{92}$$

The finite element formulation of the linearized virtual membrane strains reads

$$\begin{aligned} \Delta\delta\varepsilon_{11\alpha} &= \sum_{I}\sum_{K} D_{\lambda\mu\alpha}\, \delta\mathbf{u}^{T}_{I\lambda} \left(N_{I,1} N_{K,1}\right) \Delta\mathbf{u}_{K\mu} \\ \Delta\delta\varepsilon_{22\alpha} &= \sum_{I}\sum_{K} D_{\lambda\mu\alpha}\, \delta\mathbf{u}^{T}_{I\lambda} \left(N_{I,2} N_{K,2}\right) \Delta\mathbf{u}_{K\mu} \\ 2\Delta\delta\varepsilon_{12\alpha} &= \sum_{I}\sum_{K} D_{\lambda\mu\alpha}\, \delta\mathbf{u}^{T}_{I\lambda} \left(N_{I,1} N_{K,2} + N_{I,2} N_{K,1}\right) \Delta\mathbf{u}_{K\mu} . \end{aligned} \tag{93}$$

Equation (92) can therefore be written as

$$\Delta\delta\boldsymbol{\varepsilon}^{T}_{\alpha}\boldsymbol{\sigma}_{\alpha} = \sum_{I}\sum_{K} \delta\mathbf{v}^{T}_{I\lambda}\, \mathbf{G}_{IK\lambda\mu}\, \Delta\mathbf{v}_{K\mu} \tag{94}$$

with the integrand of the geometrical matrix defined as

$$\begin{aligned} \mathbf{G}_{IK\lambda\mu} &= D_{\lambda\mu\alpha} \begin{bmatrix} \widehat{n}_{IK\alpha}\mathbf{1}_{3\times 3} & \mathbf{0}_{3\times 3} \\ \mathbf{0}_{3\times 3} & \mathbf{0}_{3\times 3} \end{bmatrix} \\ \widehat{n}_{IK\alpha} &= N_{I,1} N_{K,1} n^{11}_{\alpha} + \left(N_{I,1} N_{K,2} + N_{I,2} N_{K,1}\right) n^{12}_{\alpha} \\ &\quad + N_{I,2} N_{K,2} n^{22}_{\alpha} \ . \end{aligned} \tag{95}$$

Analogous to the **B**-matrix, the augmented integrand can also be specified as

$$\mathbf{G}_{IK} = \begin{bmatrix} \mathbf{G}_{IK00} & \cdots & \mathbf{G}_{IK0\lambda} & \cdots & \mathbf{G}_{IK0P} \\ \vdots & \ddots & \vdots & \ddots & \vdots \\ \mathbf{G}_{IK\gamma 0} & \cdots & \mathbf{G}_{IK\lambda\mu} & \cdots & \mathbf{G}_{IK\gamma P} \\ \vdots & \ddots & \vdots & \ddots & \vdots \\ \mathbf{G}_{IKP0} & \cdots & \mathbf{G}_{IKP\lambda} & \cdots & \mathbf{G}_{IKPP} \end{bmatrix} \tag{96}$$

and hence Eq. (94) can be written compactly as

$$\Delta\delta\boldsymbol{\varepsilon}^{T}_{\alpha}\boldsymbol{\sigma}_{\alpha} = \sum_{I}\sum_{K} \delta\mathbf{v}^{T}_{I}\, \mathbf{G}_{IK}\, \Delta\mathbf{v}_{K} \ . \tag{97}$$

5.4 Transverse shear strains

Fully integration of the shear part of the tangent stiffness matrix with Eq. (88) leads to the well-known shear locking effect. In order to avoid this issue, we use the approach proposed by [31, 32]. For this reason, the shear strains γ_{13} and

γ_{23} are approximated using an independent ansatz. Within the scope of the spectral stochastic formulation, the constant-linear interpolation for one coefficient of the shear strains reads

$$\begin{bmatrix} \tilde{\gamma}_{\xi 3\gamma} \\ \tilde{\gamma}_{\eta 3\gamma} \end{bmatrix} = \frac{1}{2} \begin{bmatrix} (1-\eta)\tilde{\gamma}^{B}_{\xi 3\gamma} + (1+\eta)\tilde{\gamma}^{D}_{\xi 3\gamma} \\ (1-\xi)\tilde{\gamma}^{A}_{\eta 3\gamma} + (1+\xi)\tilde{\gamma}^{C}_{\eta 3\gamma} \end{bmatrix} \tag{98}$$

with the compatible shear strains at the collocation points defined as

$$\tilde{\gamma}^{M}_{\xi 3\gamma} = \left[x_{1,\xi}\, \beta_{1\gamma} + x_{2,\xi}\, \beta_{2\gamma} + u_{3,\xi} \right]^{M} \quad M \in \{B, D\} \ , \tag{99}$$

$$\tilde{\gamma}^{L}_{\eta 3\gamma} = \left[x_{1,\eta}\, \beta_{1\gamma} + x_{2,\eta}\, \beta_{2\gamma} + u_{3,\eta} \right]^{L} \quad L \in \{A, C\} \ . \tag{100}$$

The corresponding collocation points A, B, C, D are defined in Fig. 5. Furthermore, the Jacobian matrix, defined in Eq. (82), is used to transform the shear strains introduced with respect to ξ, η into the local Cartesian coordinate system

$$\begin{bmatrix} \gamma_{13\gamma} \\ \gamma_{23\gamma} \end{bmatrix} = \mathbf{J}^{-T} \begin{bmatrix} \tilde{\gamma}_{\xi 3\gamma} \\ \tilde{\gamma}_{\eta 3\gamma} \end{bmatrix} \ . \tag{101}$$

Within the framework of the presented quadrilateral shell element, the variations of the modified shear strains can be approximated as

$$\begin{bmatrix} \delta\gamma_{13\gamma} \\ \delta\gamma_{23\gamma} \end{bmatrix} = \sum_{I} D_{\lambda\beta\gamma}\, \bar{\mathbf{B}}^{s}_{I\beta} \begin{bmatrix} \delta u_{3\lambda} \\ \delta\beta_{1\lambda} \\ \delta\beta_{2\lambda} \end{bmatrix} \ , \tag{102}$$

with the modified matrix

$$\bar{\mathbf{B}}^{s}_{I\beta} = \mathbf{J}^{-T} \begin{bmatrix} \delta_{\beta 0} N_{I,\xi} & \delta_{\beta 0} N_{I,\xi} \xi_I x^{M}_{,\xi} & \delta_{\beta 0} N_{I,\xi} \xi_I y^{M}_{,\xi} \\ \delta_{\beta 0} N_{I,\eta} & \delta_{\beta 0} N_{I,\eta} \eta_I x^{L}_{,\eta} & \delta_{\beta 0} N_{I,\eta} \eta_I y^{L}_{,\eta} \end{bmatrix} \ . \tag{103}$$

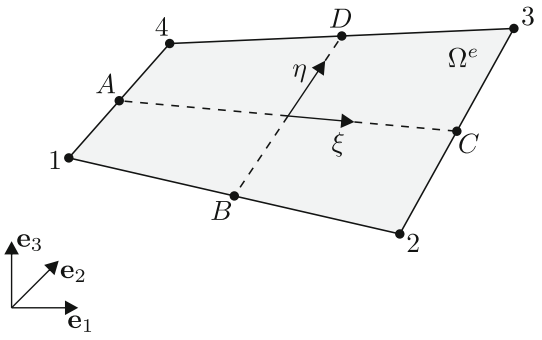

Fig. 5 Quadrilateral shell element with collocation points

In general, the local derivatives of the bi-linear ansatz functions can be written as

$$N_{I,\xi} = \frac{1}{4}\xi_I(1+\eta\eta_I) \quad N_{I,\eta} = \frac{1}{4}\eta_I(1+\xi\xi_I) \tag{104}$$

with ξ_I, η_I being the local coordinates of the corresponding node I. The collocation points are allocated to the nodal points of the element with

$$(I, M, L) \in \{(1, B, A),\ (2, B, C),\ (3, D, C),\ (4, D, A)\} \ . \tag{105}$$

A detailed derivation of the matrix shown in Eq. (103) can be found in Appendix J. With this approach, a 2×2 integration is used for all components of the residual and the tangent stiffness matrix.

5.5 Discrete form of the stochastic variational formulation

Finally, all finite element approximations can be inserted into the linearized weak form. Considering one element e, the virtual external work yields

$$\begin{aligned} \mathbb{E}\left[\delta\pi^{e}_{ext}(\omega)\right] &= \sum_{I} \delta\mathbf{v}^{T}_{I\alpha} \left(\int_{\Omega^e} N_I\, \bar{\mathbf{q}}_\alpha \, \mathrm{d}A + \int_{\partial\Omega^e} N_I\, \bar{\mathbf{f}}_\alpha \, \mathrm{d}s \right) \\ &= \sum_{I} \delta\mathbf{v}^{T}_{I} \left(\int_{\Omega^e} N_I\, \bar{\mathbf{q}} \, \mathrm{d}A + \int_{\partial\Omega^e} N_I\, \bar{\mathbf{f}} \, \mathrm{d}s \right) \\ &= \sum_{I} \delta\mathbf{v}^{T}_{I}\, \mathbf{p}_I \ . \end{aligned} \tag{106}$$

All PC coefficients of the external loads can be summarized in the vectors

$$\bar{\mathbf{q}} = \left[\bar{\mathbf{q}}^{T}_{0} \ldots \bar{\mathbf{q}}^{T}_{\alpha} \ldots \bar{\mathbf{q}}^{T}_{P} \right]^{T} , \quad \bar{\mathbf{f}} = \left[\bar{\mathbf{f}}^{T}_{0} \ldots \bar{\mathbf{f}}^{T}_{\alpha} \ldots \bar{\mathbf{f}}^{T}_{P} \right]^{T} \ . \tag{107}$$

In case of deterministic loads, only the first coefficients $\mathbf{q}_0$ and $\mathbf{f}_0$ are non-zero. At the element level, the residual is defined as the difference between the internal and external forces

$$\begin{aligned} \mathbb{E}\left[\delta\pi^{e}(\omega)\right] &= \sum_{I} \delta\mathbf{v}^{T}_{I} \left(\int_{\Omega^e} \mathbf{B}^{T}_{I}\, \boldsymbol{\sigma} \, \mathrm{d}A - \mathbf{p}_I \right) \\ &= \sum_{I} \delta\mathbf{v}^{T}_{I}\, (\mathbf{f}_I - \mathbf{p}_I) \\ &= \delta\mathbf{v}^{eT} \left(\mathbf{f}^{\,e} - \mathbf{p}^{e} \right) \\ &= \delta\mathbf{v}^{eT}\, \mathbf{g}^{e} \qquad \mathbf{g}^{e} \in \mathbb{R}^{24\tilde{P}} \ . \end{aligned} \tag{108}$$

The tangent stiffness matrix results from the consistent linearization of the residual and leads to

$$\begin{aligned}
&\mathbb{E}\left[\Delta\delta\pi^e(\omega)\right] \\
&= \sum_I \sum_K \delta\mathbf{v}_I^T \left(\int_{\Omega^e} \mathbf{B}_I^T \mathbf{D}\, \mathbf{B}_K + \mathbf{G}_{IK}\, \mathrm{d}A \right) \Delta\mathbf{v}_K \\
&= \delta\mathbf{v}^{eT} \mathbf{k}_T^e \Delta\mathbf{v}^e \qquad \mathbf{k}_T^e \in \mathbb{R}^{24\bar{P}\times 24\bar{P}} \,. \qquad (109)
\end{aligned}$$

Taking into account Eqs. (108) and (109), the complete discretization of the linearized weak form for one element reads

$$\mathrm{L}\left[\mathbb{E}\left[\delta\pi^e(\omega)\right]\right] = \delta\mathbf{v}^{eT}\left(\mathbf{g}^e + \mathbf{k}_T^e \Delta\mathbf{v}^e\right) \,. \qquad (110)$$

Equation (110) is formulated in the local coordinates of the element and must be transformed into the global coordinate system before assembling. This is done with the already defined transformation matrix, see Appendix I. The global vectors and matrices are obtained by assembling all element arrays

$$\Delta\mathbf{V} = \bigcup_{e=1}^{n_e} \Delta\tilde{\mathbf{v}}^e \,, \qquad \mathbf{G} = \bigcup_{e=1}^{n_e} \tilde{\mathbf{g}}^e \,, \qquad \mathbf{K}_T = \bigcup_{e=1}^{n_e} \tilde{\mathbf{k}}_T^e \qquad (111)$$

which leads to

$$\delta\mathbf{V}^T \left(\mathbf{K}_T \Delta\mathbf{V} + \mathbf{G}\right) = 0 \,. \qquad (112)$$

Since the virtual displacements $\delta\mathbf{V}$ are arbitrary but non-zero, we finally get the system of equations for determining the unknown displacement increment

$$\mathbf{K}_T \Delta\mathbf{V} = -\mathbf{G} \,. \qquad (113)$$

The two-step discretization procedure of the stochastic weak form in Eq. (44) leads to a system of nonlinear algebraic equations, which is solved in the context of a standard Newton iteration scheme. With the introduction of a so-called load factor λ, the global residual vector is given by

$$\mathbf{G}(\mathbf{V}, \lambda) = \mathbf{F}(\mathbf{V}) - \lambda\mathbf{P} \,, \qquad (114)$$

where $\mathbf{F}(\mathbf{V})$ is the vector of internal forces and $\mathbf{P}$ is a basic external load vector. Starting from a known equilibrium state, the unknown displacements for a given load level are calculated iteratively. In each Newton iteration step the discrete linearization in Eq. (113) has to be solved.

The developed SFEM shell element has been implemented into an extended version of the general finite element program FEAP [40].

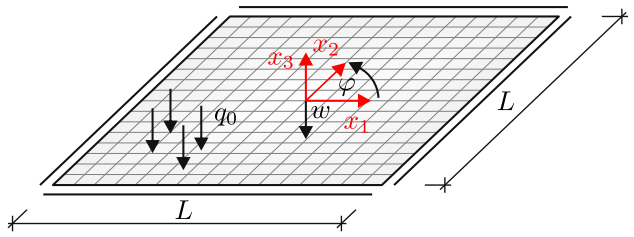

Fig. 6 Square plate under surface load

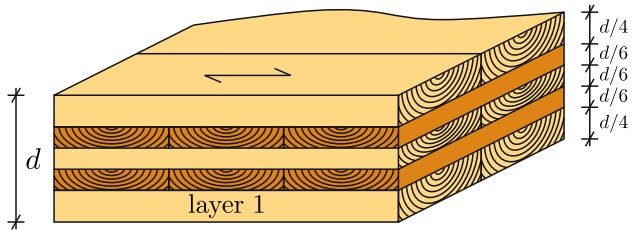

Fig. 7 Layer sequence [0° / 90° / 0° / 90° / 0°]

Table 2 Material parameters, geometrical parameters and loadings quantified as Gaussian random variables

Name	Unit	X_i	Distrib	μ_{X_i}	σ_{X_i}
$\Delta\varphi$	[°]	X_1	Gaussian	0	1.5
E_1	[kN/cm^2]	X_2	Gaussian	1160	116
E_2	[kN/cm^2]	X_2	Gaussian	39	3.9
d	[cm]	X_3	Gaussian	12	1.2
q_0	[kN/cm^2]	X_4	Gaussian	2E-4	2E-5

6 Numerical examples

6.1 Timber plate with a 5-layer cross-ply laminate

The first example is a plate with a 5-layer cross-ply laminate subjected to a constant surface load q_0. The square plate with an edge length of $L = 400$ cm and a total thickness d is simply supported (soft support) on all sides, see Fig. 6.

Transversal isotropy is assumed for the timber material behavior. The layer sequence of the cross-ply laminate plate is shown in Fig. 7. Here, 0° indicates a fiber orientation in the x_1-direction.

For the probabilistic calculation, we take into account uncertainties in material and geometrical parameters and in the surface load. The uncertain parameters are modeled as Gaussian random variables, which are characterized by their mean value μ_{X_i} and standard deviation σ_{X_i}, see Table 2.

We assume that the Young's moduli E_1 and E_2 are fully correlated. Both parameters can therefore be represented by the random variable X_2, see Table 2. The total thickness d of the shell is also modeled as a random variable. However, the ratio of the thickness of the individual layers to the total thickness, see Fig. 7, remains unchanged. In addition, the

Table 3 Settings for SFEM computation, notation, total number of polynomials $\bar{P}$ and degrees of freedom (dofs)

Settings	Notation	$\bar{P}$	dofs
$p = 0 \,/\, q = 1$	sfem $p0$	1	1253
$p = 1 \,/\, q = 1$	sfem $p1$	5	6265
$p = 2 \,/\, q = 1$	sfem $p2$	15	18795
$p = 3 \,/\, q = 1$	sfem $p3$	35	43855
$p = 4 \,/\, q = 1$	sfem $p4$	70	87710
$p = 4 \,/\, q = 0.8$	sfem $p4/q0.8$	39	48867
$p = 4 \,/\, q = 0.6$	sfem $p4/q0.6$	23	28819

surface load q_0 is modeled as a stochastic quantity. Due to the random variation $\Delta\varphi$ of the fiber orientation, the modified layer sequence results in

$$[0^\circ + \Delta\varphi \,/\, 90^\circ + \Delta\varphi \,/\, 0^\circ + \Delta\varphi \,/\, 90^\circ + \Delta\varphi \,/\, 0^\circ + \Delta\varphi] \,. \tag{115}$$

The fiber orientation of each layer is varied in the same manner. The following deterministic values are chosen for the remaining material parameters

$$G_{12} = 72 \quad \text{kN/cm}^2, \quad G_{23} = 10 \quad \text{kN/cm}^2, \quad \nu_{12} = 0.03 \,. \tag{116}$$

As a consequence of the random fiber variation, the structure has no symmetry and the calculation has to be performed on the entire system. The discretization of the structure with 16×16 shell elements results in 1253 degrees of freedom in the deterministic case, taking into account the boundary conditions. Depending on the chosen polynomial basis for the approximation of the stochastic dimensions, additional degrees of freedom arise, see Table 3.

A polynomial degree of $p = 0$ is equivalent to a deterministic simulation. The number of degrees of freedom grows significantly when the polynomial degree of the chaos expansion is increased. By considering the hyperbolic truncation scheme in Eq. (31), the number of basis polynomials $\bar{P}$ can be reduced considerably. The influence of the so-called q-norm on the calculation and on the results is examined in more detail in this numerical example.

In the simulation, the stochastic surface load q_0 is increased by the deterministic load factor λ. Here, 15 load steps with $\Delta\lambda = 1$ are used. The following diagrams depict the deterministic load factor λ versus the stochastic moments such as mean value, standard deviation or skewness of the random center displacement w.

In order to obtain accurate reference results with the Monte Carlo simulation, the number of sample points is set to 10^4. With this number of samples, the stochastic moments up to the skewness can be considered as converged. To quantify the convergence of the MCS, the stochastic moments of the center displacement w at the load step $\lambda = 5$ are considered. The convergence of the MCS results is evaluated using this quantity of interest, because it is examined in more detail later. Comparing the MCS results with 10^4 sample points with the reference solution using 5×10^5 random samples leads to a percentage error less than 2% in the skewness of this quantity of interest. In the following diagrams, the reference solution of the MCS is labeled mcs $1e4$. The results for the mean value μ_w are depicted in Fig. 8. It can be seen that the SFEM can correctly capture the mean value almost independent of the chosen polynomial degree. The standard deviation of the center displacement w is shown in Fig. 9. For a correct calculation of the standard deviation, at least a quadratic polynomial basis is required, see Fig. 9 (left). In addition, the hyperbolic truncation scheme can significantly reduce the computational effort, while the results of the standard deviation remain almost unchanged, as shown in Fig. 9 (right). Here, a linear chaos expansion is not able to describe the skewness of a random quantity. This fact can be seen in Fig. 10 (left). For the correct computation of the skewness, higher order PC expansions are necessary. In this example, at least a PCE with $p = 4$ is required, containing in total 70 polynomials. To reduce the computational costs, a hyperbolic truncation scheme should be used. A q-norm of $q = 0.6$ reduces the number of polynomials by 67.1%, but this leads to the fact that the skewness can no longer be captured correctly, especially in the range $1 \leq \lambda \leq 5$, see Fig. 10 (right). With $q = 0.8$, only 44.3% of the polynomials are omitted, which leads to a more accurate mapping of the skewness. Furthermore, Fig. 10 illustrates that the skewness decreases as the load increases. This can be explained by the increasing stiffening of the structure.

The computation time for the SFEM depends significantly on the size of the polynomial basis used for the PCE. Different numbers of degrees of freedom arise according to the chosen polynomial degree and the q-norm. For a comparison of the computational effort, the ratio between the SFEM and MCS computation time, i.e the speedup factor, is given in Table 4. For the SFEM with $p = 4$ and $q = 0.8$, which provides a good approximation quality up to the skewness, a speedup factor of 17.6 is obtained. It should be noted, that for the mean value and the standard deviation, less MCS samples are required but also a lower polynomial degree of the PC expansion is sufficient to approximate these stochastic moments. However, the speedup factors in Table 4 can be scaled, e.g., if 10^3 MCS samples for the mean value would be sufficient, sfem $p1$ would lead to a speedup factor of 149.16.

Since all quantities in the presented stochastic FE formulation are available as PC expansion, stresses and their stochastic characteristics can also be determined directly from the post-processing. We consider the random stress σ_{11} in layer 1 at the bottom of the plate, see Fig. 7. The mean

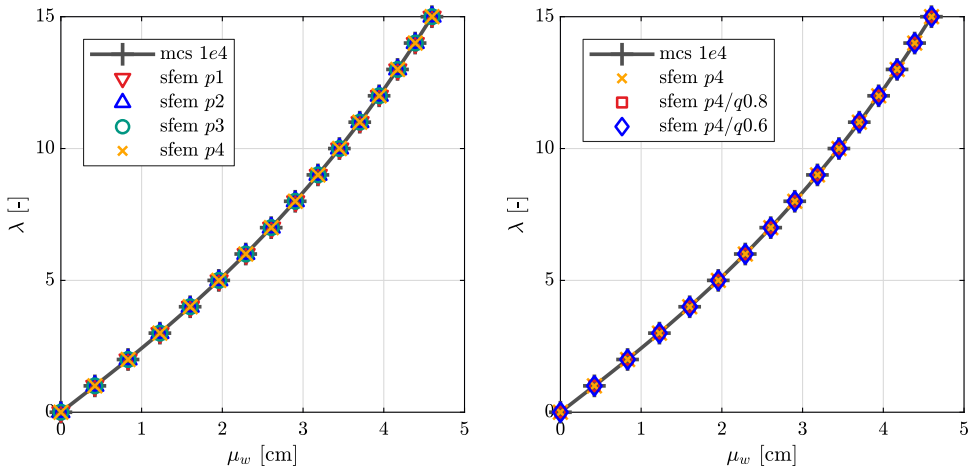

Fig. 8 Mean value μ_w of the center displacement w for several polynomial degrees of the chaos expansion

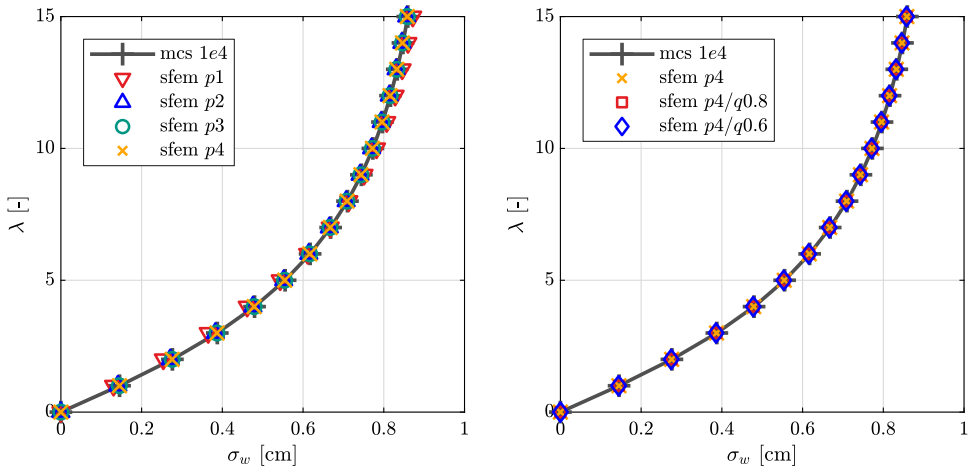

Fig. 9 Standard deviation σ_w of the center displacement w for several polynomial degrees of the chaos expansion

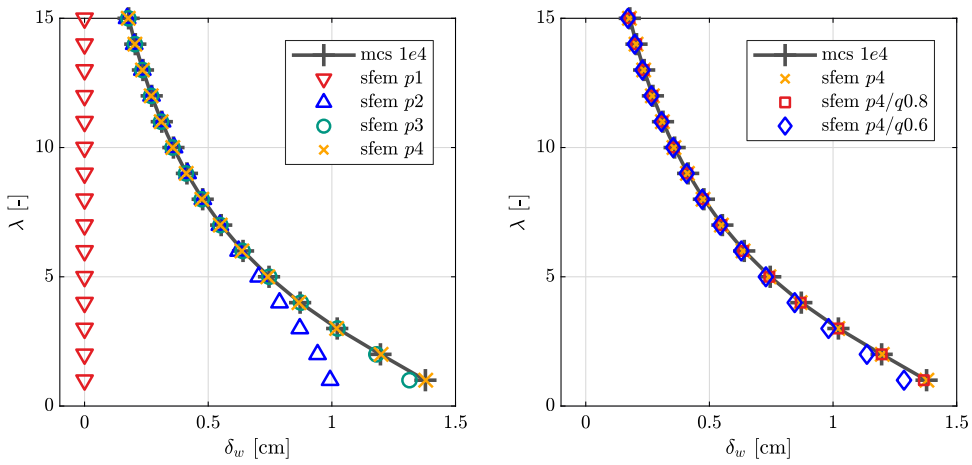

Fig. 10 Skewness δ_w of the center displacement w for several polynomial degrees of the chaos expansion

value $\mu_{\sigma_{11}}$ of σ_{11} for the load level $\lambda = 15$ is depicted in Fig. 11 and the standard deviation $\sigma_{\sigma_{11}}$ is shown in Fig. 12. For the MCS results, 10^4 random samples are used. A polynomial degree of $p = 4$ and a q-norm of $q = 0.8$ are used for the SFEM. The mean value and standard deviation of the stress σ_{11} shown in Figs. 11 and 12, are almost identical. In Table 5, the minimum and maximum values of the stress distributions are shown. The SFEM results are in very good agreement with the MCS results.

For the load step $\lambda = 4 \rightarrow \lambda = 5$, the iteration behavior is investigated. The norm of the residual vector within the equilibrium iteration is given in Table 6. Due to the consistent linearization, a quadratic convergence is achieved near equilibrium. For this example the number of iterations and

Table 4 Speedup factor: ratio between MCS and SFEM computation time $T_{\text{mcs}}/T_{\text{sfem}}$

Notation	Speedup factor
sfem $p1$	1491.6
sfem $p2$	194.4
sfem $p3$	34.2
sfem $p4$	3.1
sfem $p4/q0.8$	17.6
sfem $p4/q0.6$	82.1

Table 5 Minimum and maximum values of the mean value $\mu_{\sigma_{11}}$ and the standard deviation $\sigma_{\sigma_{11}}$ of the stress σ_{11} of the MCS and the SFEM computation

Stress value $[\text{kN/cm}^2]$	mcs $1e4$	sfem $p4/q0.8$
min. $\mu_{\sigma_{11}}$	1.286×10^{-2}	1.302×10^{-2}
max. $\mu_{\sigma_{11}}$	2.181×10^{0}	2.179×10^{0}
min. $\sigma_{\sigma_{11}}$	1.772×10^{-2}	1.750×10^{-2}
max. $\sigma_{\sigma_{11}}$	3.053×10^{-1}	3.020×10^{-1}

the norm of the residual vector are almost independent of the chosen polynomial basis of the chaos expansion.

In Fig. 13 (left), the the load factor λ versus the mean value of the center displacement w plus minus once the standard deviation is shown.

The probability density function (PDF) $f_w(w|\lambda = 5)$ of the center displacement w at the load level $\lambda = 5$ will be examined in more detail. To compute an estimate of the PDF based on a set of random samples, we use the Matlab function *ksdensity*. To obtain converged estimates of the PDF and of the quantile values of the center displacement w, 3×10^4 random samples are sufficient in this example. A percentage error less than 1% is achieved for the 99%-quantile value of the center displacement w at the load step $\lambda = 5$ compared to a reference solution with 5×10^5 MCS samples. The gray line mcs $3e4$ + fem in Fig. 13 (right) shows the reference PDF based on 3×10^4 MCS samples of the FE model. For each sample of the random variables defined in Table 2, a deterministic FE simulation has to be performed. Since the PC expansion of the center displacement w is available after the SFEM simulation is done, the PCE can be used as a surrogate model. For the dashed blue line mcs $3e4$ + sfem $p2$ and the dashed red line mcs $3e4$ + sfem $p4$ / $q0.8$ in Fig. 13 (right), the PC expansion is used to evaluate the 3×10^4 MCS samples of the random input variables. The estimated probability density functions of the MCS with the FE model and of the MCS with the SFEM show very good agreement.

Furthermore, quantile values of the center displacement w can be determined based on the 3×10^4 MCS samples. The results of the MCS with the FE model and the MCS with the SFEM are shown in Table 7. With the quadratic PC expansion, the 95 %-quantile $w_{0.95}$ of the center displacement w is approximated with an error $\varepsilon_{w_{0.95}}$ less than 1 %. The error decreases for the PCE with $p = 4$ and $q = 0.8$, see Table 7. A similar approximation behavior of the PC expansion is observed for the 99 %-quantile $w_{0.99}$ of the center displacement w, whereby the SFEM results have an error $\varepsilon_{w_{0.99}}$ between 1 % − 2 %.

Table 6 Convergence behavior for load step $\lambda = 4 \rightarrow \lambda = 5$

No. of iter	$p1$	$p2$	$p3$
1	1.884E+00	1.884E+00	1.884E+00
2	1.959E+00	1.931E+00	1.930E+00
3	2.336E-03	3.174E-03	3.140E-03
4	2.750E-08	1.032E-07	1.735E-07
5	6.940E-12	7.486E-12	6.483E-12
No. of iter	$p4$	$p4/q0.8$	$p4/q0.6$
1	1.884E+00	1.884E+00	1.884E+00
2	2.194E+00	1.931E+00	1.931E+00
3	4.234E-03	3.083E-03	3.076E-03
4	6.347E-07	1.528E-07	1.646E-07
5	5.979E-12	6.895E-12	6.160E-12

Table 7 Quantile values of the center displacement w at the load level $\lambda = 5$

Quantile values	mcs $3e4$ + fem	mcs $3e4$ + sfem $p2$	mcs $3e4$ + sfem $p4/q0.8$
$w_{0.95}$[cm]	2.9805	2.9658	2.9800
$\varepsilon_{w_{0.95}}$[%]	–	0.4932	0.0143
$w_{0.99}$[cm]	3.5652	3.5055	3.5185
$\varepsilon_{w_{0.99}}$[%]	–	1.6759	1.3105

6.2 Cylindrical composite shell panel

We investigate a cylindrical composite shell panel subjected to a concentrated load, which is a typical numerical example in geometric nonlinear shell analysis, see [41, 42]. The structure is hinged (soft support) at the two straight edges, while the two curved edges are free. The shell has the layer sequence [0° / 90° / 0°], where each layer has a thickness of $d/3$, resulting in a total thickness d. As depicted in Fig. 14, 0° indicates the circumferential direction and 90° the length direction of the shell panel.

For the probabilistic simulation, we consider uncertainties in the material and in the geometrical properties. In Table 8, the Gaussian distributed random variables are characterized by their mean value μ_{X_i} and standard deviation σ_{X_i}. In order

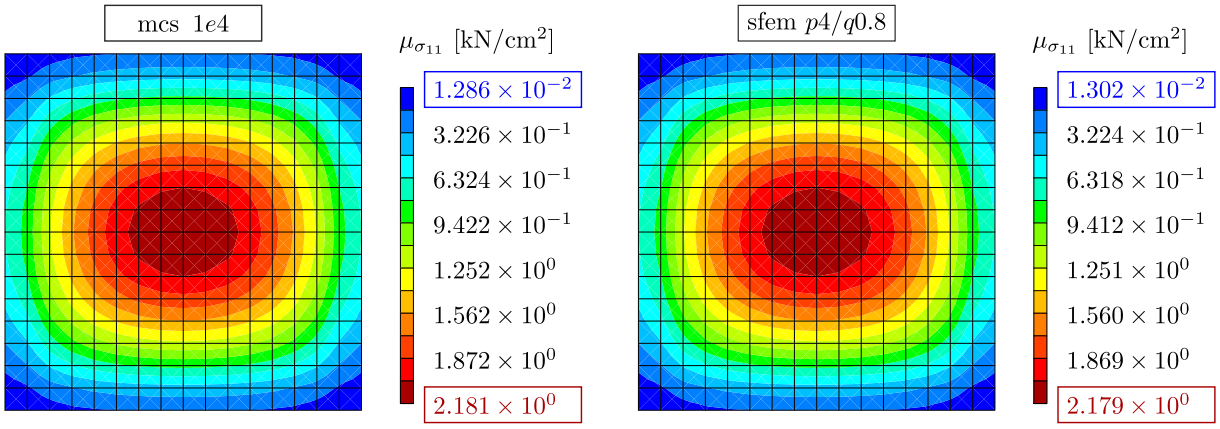

Fig. 11 Mean value $\mu_{\sigma_{11}}$ of the stress σ_{11} at the bottom of layer 1: (left) mcs $1e4$, (right) sfem $p4/q0.8$

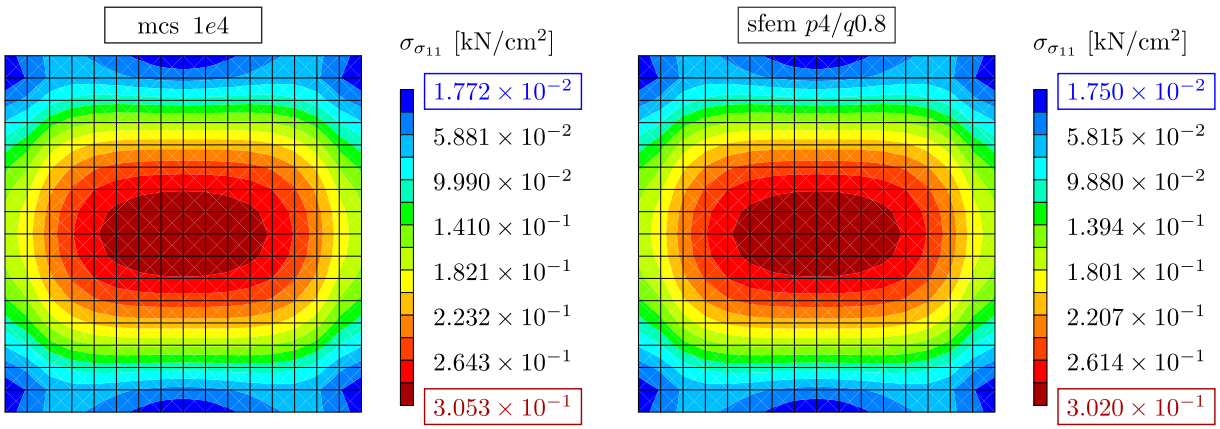

Fig. 12 Standard deviation $\sigma_{\sigma_{11}}$ of the stress σ_{11} at the bottom of layer 1: (left) mcs $1e4$, (right) sfem $p4/q0.8$

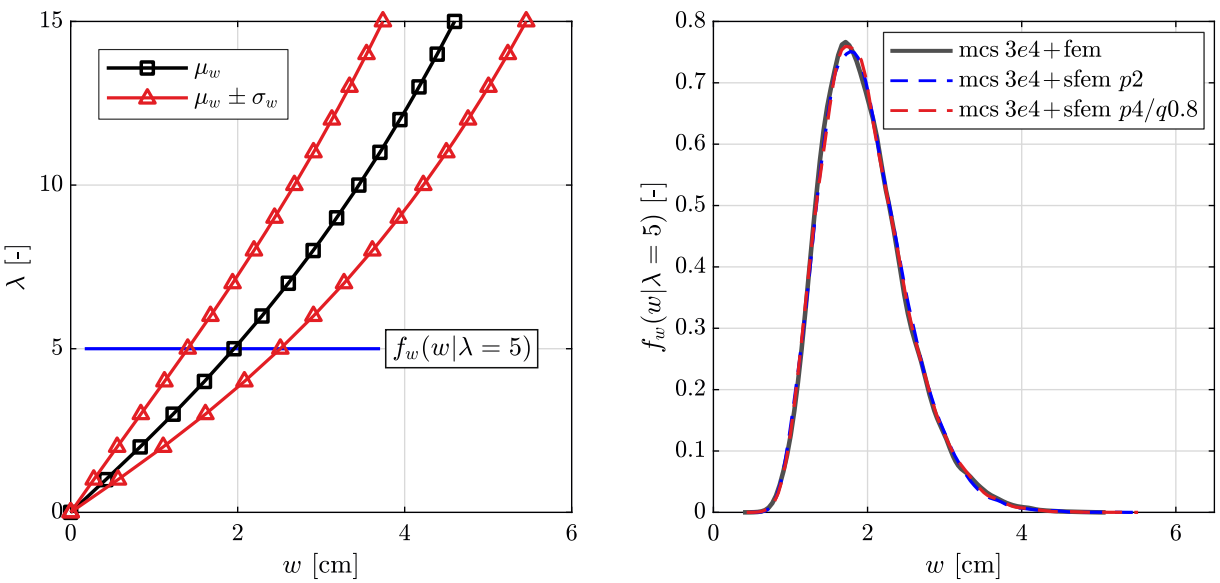

Fig. 13 Left: mean value μ_w plus minus standard deviation σ_w of the center displacement w, right: PDF of the center displacement w at load level $\lambda = 5$

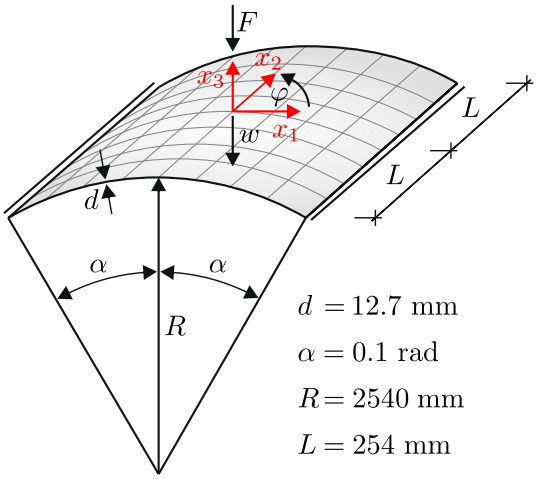

Fig. 14 Cylindrical composite shell panel and geometrical parameters

Table 8 Material parameters and geometrical parameters quantified as Gaussian and uniform random variables

Name	Unit	X_i	Distrib	μ_{X_i}/a_{X_i}	σ_{X_i}/b_{X_i}
$\Delta\varphi$	[°]	X_1	Gaussian	0	1.5
E_1	[N/mm^2]	X_2	Gaussian	3300	330
E_2	[N/mm^2]	X_2	Gaussian	1100	110
d	[mm]	X_3	Uniform	11.2	14.2

Table 9 Settings for SFEM computation, notation, total number of polynomials $\bar{P}$ and degrees of freedom (dofs)

Settings	Notation	$\bar{P}$	dofs
$p = 0\,/\,q = 1$	sfem $p0$	1	414
$p = 1\,/\,q = 1$	sfem $p1$	4	1656
$p = 2\,/\,q = 1$	sfem $p2$	10	4140
$p = 3\,/\,q = 1$	sfem $p3$	20	8280
$p = 4\,/\,q = 1$	sfem $p4$	35	14490

to define the uniform distribution in Table 8, the lower bound a_{X_i} and the upper bound b_{X_i} are used.

Similar to the first example, see Sect. 6.1, we assume that E_1 and E_2 are fully correlated. Both parameters can thus be described by the random variable X_2. The thickness d of the shell has a large influence on the structural behavior of the panel. We model this parameter by a uniform distribution. However, the ratio between the individual layer thicknesses and the overall thickness remains unchanged. Since we assume that the fiber orientations of the layers are uncertain, the numerical model has no symmetry and the simulation is performed on the entire system. The random variation $\Delta\varphi$ of the fiber orientation yields the modified stacking sequence

$$[0° + \Delta\varphi/90° + \Delta\varphi/0° + \Delta\varphi]. \tag{117}$$

In this example, the input parameters in Table 8 include both normal and uniform distributions. In total, there are three independent random variables, therefore three-dimensional polynomials are used for the stochastic discretization. The approximation in the X_1- and X_2-direction is performed with Hermite polynomials, while Legendre polynomials are used for the X_3-direction, see Table 1. All remaining material parameters of the structure are assumed to be deterministic with the following values

$$G_{12} = 660 \ \text{N/mm}^2, \quad G_{23} = 450 \ \text{N/mm}^2, \quad \nu_{12} = 0.25\,. \tag{118}$$

For the numerical simulation, the structure is discretized with 8×8 shell elements. In the case of a deterministic analysis, this results in a total of 414 degrees of freedom. Table 9 lists the total number of the resulting degrees of freedom depending on the chosen polynomial degree and the q-norm.

This example is more challenging since a snap-through behavior of the structure occur, see the load–displacement behavior in Fig. 15. Therefore all numerical simulations are carried out displacement controlled. The center displacement w is increased in steps of $\Delta w = 1$ mm from 0 to 30 mm and the reaction force F is calculated. Accurate results with the Monte Carlo simulation are obtained by using 10^4 sample points. In order to determine the quality of the MCS results, the stochastic moments of the reaction force at the displacement level $w = 20$ are considered. Since the reaction force at this displacement level is examined in more detail later, the convergence of the MCS results is quantified using this variable. With 10^4 random samples, a percentage error in the skewness less than 3% is achieved compared to a reference result with 5×10^5 MCS samples. The results of the MCS are labeled mcs $1e4$ in the diagrams. In the case of a displacement control within the framework of the SFEM, the controlled displacement is deterministic. Therefore the following diagrams, depict stochastic quantities of interest such as mean value, standard deviation and skewness of the reaction force F versus the deterministic center displacement w.

As shown in Fig. 15, the SFEM can capture the mean value μ_F of the reaction force F for all investigated polynomial degrees with a high agreement. A similar approximation behavior can be observed for the standard deviation of the reaction force, see Fig. 16. However, a linear polynomial approximation is not able to describe the skewness of the reaction force, see Fig. 17. With increasing polynomial degree, a very good agreement between the results of the SFEM and the MCS can be achieved. It is notable that a slightly worse approximation of the skewness can be seen for the displacement level $w = 19$ and $w = 20$. In this range, the values of the reaction force change significantly, as the structure has passed the limit point and snaps through. A higher polynomial degree is required to capture higher-

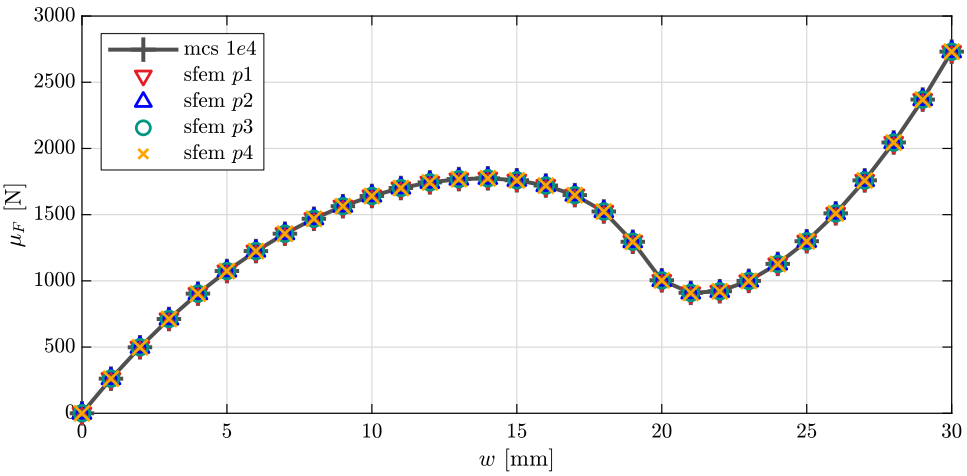

Fig. 15 Mean value μ_F of the reaction force F for several polynomial degrees of the chaos expansion

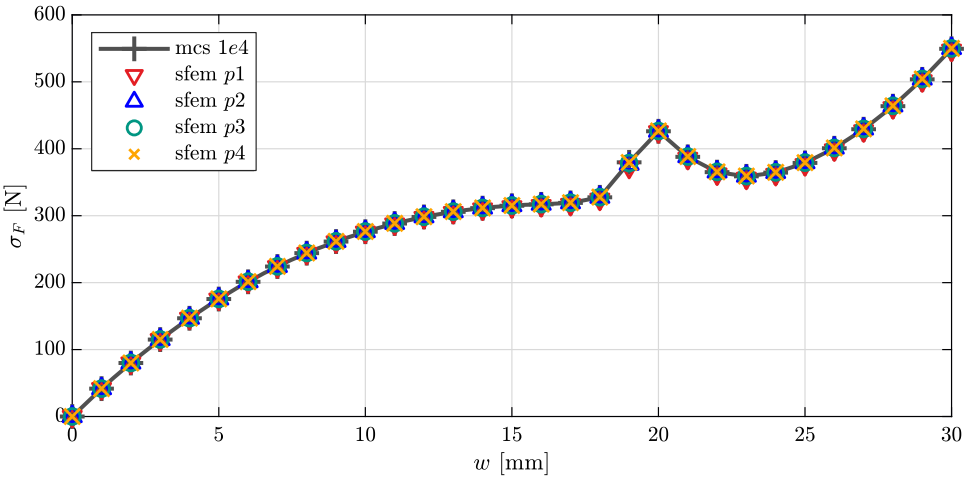

Fig. 16 Standard deviation σ_F of the reaction force F for several polynomial degrees of the chaos expansion

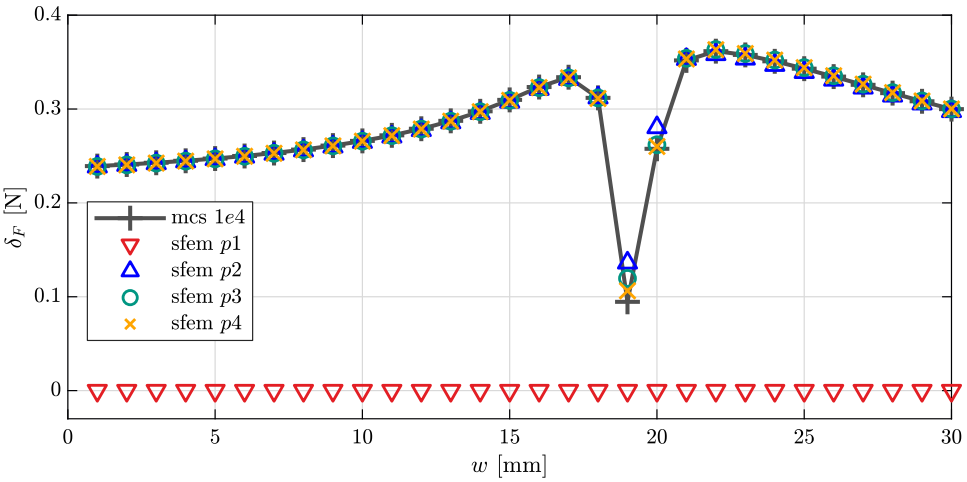

Fig. 17 Skewness δ_F of the reaction force F for several polynomial degrees of the chaos expansion

order stochastic moments at these displacement levels almost exactly.

Considering the convergence behavior for the displacement step $w = 19 \rightarrow w = 20$, see Table 10, it can be seen that one more iteration is necessary as the polynomial degree increases. However, a quadratic convergence occurs near equilibrium.

For a comparison of the computational effort, the speedup factor in Table 11 is considered. Similar to the first example, the computation time for the SFEM depends significantly on the polynomial degree of the PCE. With an increasing poly-

Table 10 Convergence behavior for the displacement step $w = 19 \rightarrow w = 20$

No. of iter	$p2$	$p3$	$p4$
1	2.649E+05	2.649E+05	2.649E+05
2	1.490E+03	1.693E+03	1.822E+03
3	7.328E+01	1.014E+02	1.166E+02
4	4.684E+01	8.809E+01	1.083E+02
5	1.062E+00	4.438E+00	8.273E+00
6	4.063E-03	1.122E-01	5.145E-01
7	2.182E-08	2.615E-05	5.554E-04
8	Conv	2.159E-09	4.003E-09
9		Conv	Conv

Table 11 Speedup factor: ratio between MCS and SFEM computation time $T_{\text{mcs}}/T_{\text{sfem}}$

Notation	Speedup factor
sfem $p1$	1968.0
sfem $p2$	676.8
sfem $p3$	187.6
sfem $p4$	51.9

nomial basis, the speedup factor decreases significantly. The SFEM with $p = 4$ is 51.9 times faster than the MCS and provides good approximations up to the skewness. Similar to the first example in Sect. 6.1, fewer MCS samples are required for the stochastic moments such as the the mean value and the standard deviation, while a lower polynomial degree of the SFEM is also sufficient. The speedup factors in Table 11 can be scaled as described in Sect. 6.1.

For this example, we assume uncertainties in the material and geometrical parameters, see Table 8. Since the center displacement w is controlled, this degree of freedom is deterministic. All other displacements are in general not deterministic. A quantity that is uncertain is the reaction force F, see Fig. 14. This behavior can be observed in Fig. 18 (left), which shows the mean value μ_F plus minus once the standard deviation σ_F of the reaction force F plotted as a function of the deterministic center displacement w.

Finally, the probability density function $f_F(F|w = 20)$ of the reaction force F at the displacement level $w = 20$ is shown in Fig. 18 (right). The computation of the probability density function $f_F(F|w = 20)$ is performed in the same way as described in Sect. 6.1. With 3×10^4 MCS samples, a converged estimate of the probability density function is achieved. The convergence of the MCS results is examined in the same way as in the first example, see Sect. 6.1. It can be observed that the quadratic chaos expansion is not able to approximate the MCS results with good agreement. Increasing the polynomial degree to $p = 4$ provides a very good approximation of the estimated PDF.

7 Conclusion and outlook

In this paper, a spectral stochastic finite element formulation for geometric nonlinear composite shells has been presented. Based on the stochastic variational formulation, a two-step discretization scheme for the stochastic displacement field has been introduced. The stochastic space is discretized with the PCE, while the spatial discretization is performed with

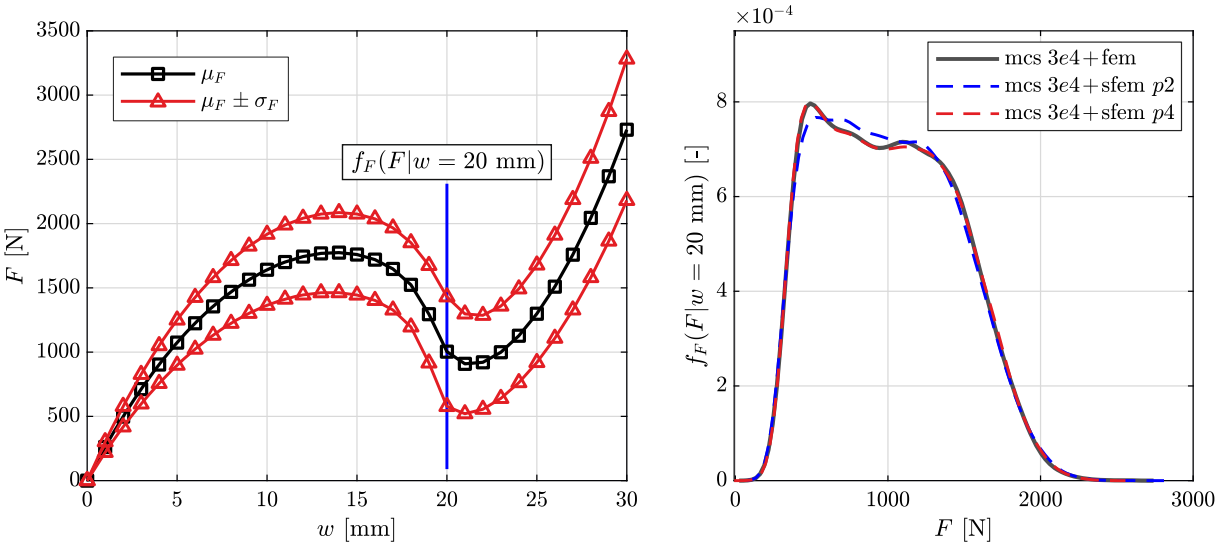

Fig. 18 Left: mean value μ_F plus minus standard deviation σ_F of the reaction force F, right: PDF of the reaction force F at the displacement level $w = 20$ mm

the FEM. Subsequently, the developed spectral stochastic FE formulation has been applied to two numerical examples.

We investigated geometric nonlinear composite shells subjected to uncertain material and geometrical parameters as well as stochastic loadings. It has been shown, that the developed stochastic shell formulation is able to approximate the random structural response. Results of the SFEM and the MCS show excellent agreement. Within the method, all stochastic quantities are characterized by their PC coefficients. During the post-processing, stochastic moments of displacements, reaction forces and also stresses can be determined at low computational cost. The hyperbolic truncation scheme from [8] has been applied in the context of the SFEM to avoid the exponential increase of the polynomial basis in problems with multiple random variables. The studies have shown that the polynomial degree of the PCE has a significant influence on the quality of the results, but also on the computation time. Investigations indicated, that the consistent linearization of the equations results in a quadratic convergence in the vicinity of the equilibrium point within the Newton iteration. Furthermore, a computation with the SFEM provides a surrogate model that can additionally be used in combination with the MCS to obtain a high number of samples of the quantities of interest, which can be used to estimate the corresponding density functions or to compute quantile values for structural reliability analysis. Investigations concerning the computation times have shown that the speedup factor depends mainly on the chosen polynomial degree and on the number of random input variables. For the problems investigated here, it was shown that the SFEM is significantly faster than the MCS.

In addition to the advantages that the SFEM provides, the method has some drawbacks. The total number of degrees of freedom depends significantly on the investigated problem and on the number of basis polynomials. The exponential increase of the polynomial basis for problems with several random variables leads to more unknowns and larger systems of equations to solve, which has influence on the computation time. In the MCS a parallelization can reduce the computational effort, because all random samples are calculated independently of each other. Within the scope of the SFEM, such a parallelization is not possible. However, the element loop can be parallelized analogously to the FEM, see [43].

A spectral stochastic formulation has been presented including a universal notation, that provides a consistent formula of the residual and the tangent stiffness matrix. Therefore, the formulation provides a straightforward implementation of the method into an existing finite element analysis program. Furthermore, standard solution algorithms, such as load control or single displacement control, can be used to trace the equilibrium path.

In future research work, the application of the method to nonlinear mixed finite element formulations, based on Hellinger-Reissner or Hu-Washizu functionals shall be investigated.

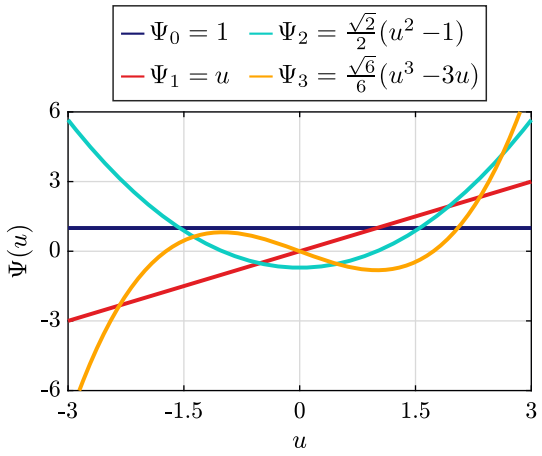

Fig. 19 Hermite polynomials

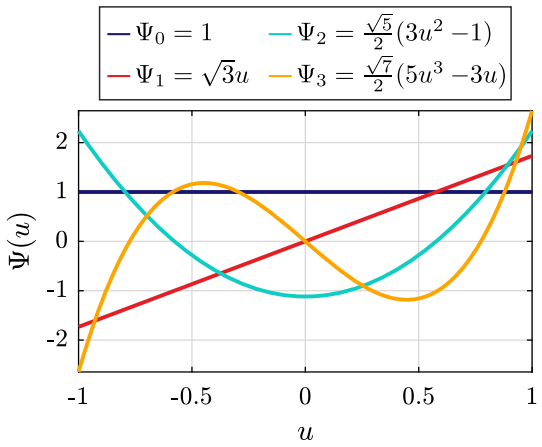

Fig. 20 Legendre polynomials

A PC expansions of normal and uniform distributions

Normal or uniform distributions are often used for modeling random variables. Since these quantities are usually not standardized, they have to be transformed into standard distributions using an isoprobabilistic transformation [44] written as

$$X = T(U)\,. \tag{119}$$

The variable U follows distributions such as standard normal $\mathcal{N}(0, 1)$ or standard uniform $\mathcal{U}(-1, 1)$, depending on the distribution of the random variable X. An exact representation of X is given by the PCE using a constant and a linear

polynomial term

$$X = \widehat{x} = \sum_{\alpha=0}^{1} x_\alpha \Psi_\alpha(U) = x_0\Psi_0(U) + x_1\Psi_1(U)\,. \tag{120}$$

If we consider the random variable $X \sim \mathcal{N}(\mu, \sigma)$, the transformation is given by

$$X = T(U) = \mu + \sigma \cdot U \qquad U \sim \mathcal{N}(0,1) \tag{121}$$

and the coefficients of the corresponding Hermite polynomials can be specified as

$$x_0 = \mu, \quad x_1 = \sigma, \quad x_\alpha = 0 \quad \forall \alpha > 1\,. \tag{122}$$

Figure 19 shows the first four orthonormal Hermite polynomials.

For a uniform distribution $X \sim \mathcal{U}(a, b)$, it follows

$$X = T(U) = \frac{a+b}{2} + \frac{b-a}{2} \cdot U \qquad U \sim \mathcal{U}(-1,1)\,, \tag{123}$$

with the coefficients of the Legendre polynomials

$$x_0 = \frac{a+b}{2}, \quad x_1 = \frac{b-a}{2\sqrt{3}}, \quad x_\alpha = 0 \quad \forall \alpha > 1\,. \tag{124}$$

The first four orthonormal Legendre polynomials are depicted in Fig. 20.

B Multiplication tensor

Analytical solutions can be given for the expected value of a triple product of polynomials. When using Hermite polynomials, the multiplication tensor is given by [45]

$$D_{\alpha\beta\gamma} = \frac{\mathbb{E}\left[\Psi_\alpha \Psi_\beta \Psi_\gamma\right]}{\mathbb{E}\left[\Psi_\gamma \Psi_\gamma\right]} = \begin{cases} \frac{\sqrt{\alpha!\beta!\gamma!}}{(k-\alpha)!(k-\beta)!(k-\gamma)!}, & \alpha+\beta+\gamma = 2k \\ & \alpha,\beta,\gamma \le k \\ 0, & \text{Otherwise}\,. \end{cases} \tag{125}$$

In the case of Legendre polynomials, the third-order tensor is calculated analytically, see [46]

$$D_{\alpha\beta\gamma} = \frac{\mathbb{E}\left[\Psi_\alpha \Psi_\beta \Psi_\gamma\right]}{\mathbb{E}\left[\Psi_\gamma \Psi_\gamma\right]} = \begin{cases} \frac{\sqrt{(2\alpha+1)(2\beta+1)(2\gamma+1)}}{(2k+1)} \\ \cdot \frac{k!^2 (2k-2\alpha)!(2k-2\beta)!(2k-2\gamma)!}{(2k)!(k-\alpha)!^2(k-\beta)!^2(k-\gamma)!^2}, & \alpha+\beta+\gamma = 2k \\ & k \in \mathbb{N}_0 \\ & \alpha,\beta,\gamma \le k \\ 0, & \text{Otherwise}\,. \end{cases} \tag{126}$$

The multiplication tensor is solely dependent on the polynomials used and can therefore be determined once before a calculation. Furthermore, the tensor has several symmetry properties

$$D_{\alpha\beta\gamma} = D_{\alpha\gamma\beta} = D_{\beta\alpha\gamma} = D_{\beta\gamma\alpha} = D_{\gamma\alpha\beta} = D_{\gamma\beta\alpha}\,. \tag{127}$$

With the orthonormality property (26) of the polynomials and the general definition of the first polynomial $\Psi_0 = 1$, it follows

$$D_{\alpha\beta 0} = \delta_{\alpha\beta} = D_{\alpha\beta\gamma}\,\delta_{\gamma 0}\,. \tag{128}$$

C Multiplication of two PC variables

We consider two normal distributions $X_1 \sim \mathcal{N}(1,1)$ and $X_2 \sim \mathcal{N}(2, 0.5)$. They can be written in terms of standard normal distributed random variables

$$X_1 = \mu_1 + \sigma_1 \cdot U_1\,, \qquad X_2 = \mu_2 + \sigma_2 \cdot U_2\,. \tag{129}$$

The multiplication of X_1 and X_2 results in the new random variable

$$Z = X_1 \cdot X_2\,. \tag{130}$$

Due to the simple arithmetic operation in Eq. (130), analytical solutions for the stochastic moments can be derived

$$\begin{aligned} \mu_Z &= \mu_1\mu_2 = 2\,, \\ \sigma_Z &= \sqrt{(\mu_1\sigma_2)^2 + (\mu_2\sigma_1)^2 + (\sigma_1\sigma_2)^2} = \frac{3\sqrt{2}}{2}\,, \\ \delta_Z &= \frac{6\mu_1\sigma_2\mu_2\sigma_1\sigma_1\sigma_2}{\sqrt{(\mu_1\sigma_2)^2 + (\mu_2\sigma_1)^2 + (\sigma_1\sigma_2)^2}^3} = \frac{2\sqrt{2}}{9}\,. \end{aligned} \tag{131}$$

Equation (131) shows that the random variable Z no longer satisfies a normal distribution. In contrast to the input variables defined in Eq. (129), the variable Z is characterized by skewness. This fact can be clearly illustrated with the corresponding PC expansions. Two-dimensional Hermite polynomials depending on the standard normal distributions

Table 12 Polynomial basis and multi-indices

α	$\mathbf{m}_\alpha$	$\Psi_\alpha(U_1, U_2)$
0	[0, 0]	$\Psi_0 = 1$
1	[0, 1]	$\Psi_1 = U_2$
2	[1, 0]	$\Psi_2 = U_1$
3	[0, 2]	$\Psi_3 = \sqrt{2}/2\,(U_2^2 - 1)$
4	[2, 0]	$\Psi_4 = \sqrt{2}/2\,(U_1^2 - 1)$
5	[1, 1]	$\Psi_5 = U_1 U_2$

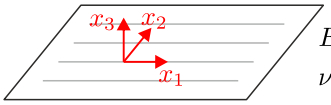

$$E_2 = 1100\ \mathrm{N/mm^2}$$
$$\nu_{12} = 0.25$$
$$E_1(\omega) \sim \mathcal{N}(3300{,}330)\ \mathrm{N/mm^2}$$

Fig. 21 Single layer and corresponding material parameters

U_1 and U_2 are used for the PC expansion of X_1 and X_2

$$X_1 = \widehat{x}_1 = \sum_{\alpha=0}^{P} x_{1\alpha}\Psi_\alpha\,, \qquad X_2 = \widehat{x}_2 = \sum_{\alpha=0}^{P} x_{2\alpha}\Psi_\alpha\,. \quad (132)$$

Choosing a total degree of $p = 2$, results in a polynomial basis containing $\bar{P} = 6$ terms. All polynomials and associated multi-indices are shown in Table 12.

The corresponding PC coefficients for the expansions in Eq. (132) can be obtained using Eq. (122). All values are summarized in the vectors

$$\mathbf{x}_1 = \left[1,\ 0,\ 1,\ 0,\ 0,\ 0\right]^T\,,\ \mathbf{x}_2 = \left[2,\ 0.5,\ 0,\ 0,\ 0,\ 0\right]^T\,. \quad (133)$$

The non-zero coefficients in Eq. (133) refer to the constant and linear polynomials. For the exact PC expansion of the random variable Z, the bilinear polynomial Ψ_5 is also required, which leads to the associated coefficient z_5 being non-zero. The PC expansion of Z is given by

$$Z = \widehat{z} = \sum_{\alpha=0}^{P} z_\alpha \Psi_\alpha\,, \qquad \mathbf{z} = \left[2,\ 0.5,\ 2,\ 0,\ 0,\ 0.5\right]^T\,. \quad (134)$$

The coefficients are determined using the formula in Eq. (38). Using Eq. (42), the mean value and the standard deviation can be determined directly from the PC expansion, given in Eq. (134)

$$\mu_{\widehat{z}} = z_0 = 2\,, \quad (135)$$

$$\sigma^2_{\widehat{z}} = \sqrt{\sum_{\alpha=1}^{P} z_\alpha^2} = \sqrt{2^2 + 0.5^2 + 0.5^2} = \frac{3\sqrt{2}}{2}\,. \quad (136)$$

The skewness can also be derived analytically using Eq. (43)

$$\delta_{\widehat{z}} = \frac{1}{\sigma^3_{\widehat{z}}} \sum_{\alpha=1}^{P}\sum_{\beta=1}^{P}\sum_{\gamma=1}^{P} D_{\alpha\beta\gamma}\, z_\alpha\, z_\beta\, z_\gamma = \frac{2\sqrt{2}}{9}\,. \quad (137)$$

Since all PC expansions shown in this section are exact, the resulting stochastic moments from the PCE in Eq. (134) match to the analytical solutions shown in Eq. (131).

D Multiplication and division of PC variables

The multiplication (38) of two PC variables can be formulated as a linear system of equations for the unknown coefficients

$$\begin{bmatrix} a_0 \\ \vdots \\ a_P \end{bmatrix} = \begin{bmatrix} D_{\alpha 00}\, b_\alpha & \cdots & D_{\alpha 0P}\, b_\alpha \\ \vdots & D_{\alpha\beta\gamma}\, b_\alpha & \vdots \\ D_{\alpha P0}\, b_\alpha & \cdots & D_{\alpha PP}\, b_\alpha \end{bmatrix} \begin{bmatrix} c_0 \\ \vdots \\ c_P \end{bmatrix}\,. \quad (138)$$

In vector–matrix notation, the multiplication reads

$$\mathbf{a} = \mathbf{B}\,\mathbf{c} \quad \mathbf{a}, \mathbf{c} \in \mathbb{R}^{\bar{P}}, \quad \mathbf{B} \in \mathbb{R}^{\bar{P}\times\bar{P}}\,. \quad (139)$$

In the case of division (40), the following relations are obtained

$$\begin{bmatrix} D_{\alpha 00}\, b_\alpha & \cdots & D_{\alpha 0P}\, b_\alpha \\ \vdots & D_{\alpha\beta\gamma}\, b_\alpha & \vdots \\ D_{\alpha P0}\, b_\alpha & \cdots & D_{\alpha PP}\, b_\alpha \end{bmatrix} \begin{bmatrix} a_0 \\ \vdots \\ a_P \end{bmatrix} = \begin{bmatrix} c_0 \\ \vdots \\ c_P \end{bmatrix} \quad (140)$$

and in short form we get

$$\mathbf{a} = \mathbf{B}^{-1}\,\mathbf{c} \quad \mathbf{a}, \mathbf{c} \in \mathbb{R}^{\bar{P}}, \quad \mathbf{B} \in \mathbb{R}^{\bar{P}\times\bar{P}}\,. \quad (141)$$

E PC expansion of the material matrix for a single layer

Due to the stochastic modeling of material parameters such as the Young's modulus, the material matrix in Eq. (15) is a stochastic quantity. Based on the PC expansion of the stochastic material properties, the corresponding PC coefficients of the material matrix can be determined considering the arithmetic operations for PC variables. This uncertainty propagation is shown with an illustrative example. Therefore we consider a single layer with the following material parameters, see Fig. 21.

In the following example, only the stiffness entry C_{12} of the material matrix $\bar{\mathbf{C}}_m$, see Eq. (15), will be considered. The analytical relationship between the Young's modulus $E_1(\omega)$

Table 13 PC coefficients of the random stiffness $C_{12}(\omega)$

$C_{12\alpha}$	$p=1$	$p=2$	$p=3$
C_{120}	280.9127	280.9141	280.9141
C_{121}	−0.6039	−0.6169	−0.6173
C_{122}	0	0.0892	0.0920
C_{123}	0	0	−0.0163

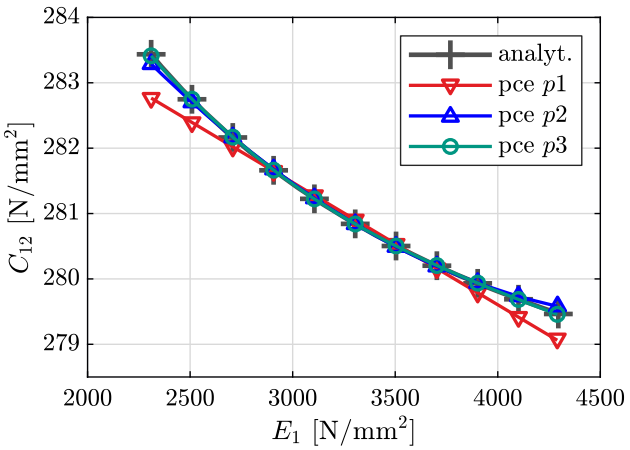

Fig. 22 Analytical relationship and polynomial approximations

and the stiffness $C_{12}(\omega)$ is given by

$$C_{12}(\omega) = C_{12}(E_1(\omega)) = \frac{\nu_{12} E_2}{1 - \dfrac{\nu_{12}^2 E_2}{E_1(\omega)}} = \frac{275}{1 - \dfrac{68.75}{E_1(\omega)}} \,. \tag{142}$$

For the polynomial approximation of the relation (142), we start with the PC expansion of the input variable

$$E_1(\omega) = \sum_{\alpha=0}^{P} E_{1\alpha} \Psi_\alpha$$
$$E_{10} = 3300, \quad E_{11} = 330, \quad E_{1\alpha} = 0 \quad \forall\, \alpha > 1 \,. \tag{143}$$

Similarly, we formulate the PCE of the output quantity

$$C_{12}(\omega) = \sum_{\alpha=0}^{P} C_{12\alpha} \Psi_\alpha \,. \tag{144}$$

Due to the normal distribution of $E_1(\omega)$, Hermite polynomials are used for the chaos expansions of the input and output variables. Table 13 shows the coefficients $C_{12\alpha}$ for different polynomial degrees of the PC expansion.

To illustrate the approximation, the analytical relationship (142) and the corresponding PC expansions (144) are shown in Fig. 22.

One can see that the cubic polynomial approximation can almost exactly describe the analytical function.

F Variation of stochastic shell strains

The variation of the remaining shell strains can be determined as follows.

$$\begin{aligned}
\delta\varepsilon_{22\gamma} &= \frac{\partial \varepsilon_{22\gamma}}{\partial u_{1\lambda,2}} \delta u_{1\lambda,2} + \frac{\partial \varepsilon_{22\gamma}}{\partial u_{2\lambda,2}} \delta u_{2\lambda,2} + \frac{\partial \varepsilon_{22\gamma}}{\partial u_{3\lambda,2}} \delta u_{3\lambda,2} \\
&= D_{\alpha\beta\gamma} \delta_{\alpha\lambda} u_{1\beta,2} \delta u_{1\lambda,2} \\
&\quad + \left(\delta_{\gamma\lambda} + D_{\alpha\beta\gamma} \delta_{\alpha\lambda} u_{2\beta,2}\right) \delta u_{2\lambda,2} \\
&\quad + D_{\alpha\beta\gamma} \delta_{\alpha\lambda} u_{3\beta,2} \delta u_{3\lambda,2} \\
&= D_{\lambda\beta\gamma} \left[u_{1\beta,2} \delta u_{1\lambda,2} + \left(\delta_{\beta 0} + u_{2\beta,2}\right) \delta u_{2\lambda,2} \right. \\
&\quad \left. + u_{3\beta,2} \delta u_{3\lambda,2} \right]
\end{aligned} \tag{145}$$

$$\begin{aligned}
2\delta\varepsilon_{12\gamma} &= \frac{2\partial \varepsilon_{12\gamma}}{\partial u_{1\lambda,1}} \delta u_{1\lambda,1} + \frac{2\partial \varepsilon_{12\gamma}}{\partial u_{1\lambda,2}} \delta u_{1\lambda,2} + \frac{2\partial \varepsilon_{12\gamma}}{\partial u_{2\lambda,1}} \delta u_{2\lambda,1} \\
&\quad + \frac{2\partial \varepsilon_{12\gamma}}{\partial u_{2\lambda,2}} \delta u_{2\lambda,2} + \frac{2\partial \varepsilon_{12\gamma}}{\partial u_{3\lambda,1}} \delta u_{3\lambda,1} + \frac{2\partial \varepsilon_{12\gamma}}{\partial u_{3\lambda,2}} \delta u_{3\lambda,2} \\
&= D_{\alpha\beta\gamma} \delta_{\alpha\lambda} u_{1\beta,2} \delta u_{1\lambda,1} \\
&\quad + \left(\delta_{\gamma\lambda} + D_{\alpha\beta\gamma} \delta_{\alpha\lambda} u_{1\beta,1}\right) \delta u_{1\lambda,2} \\
&\quad + \left(\delta_{\gamma\lambda} + D_{\alpha\beta\gamma} \delta_{\alpha\lambda} u_{2\beta,2}\right) \delta u_{2\lambda,1} \\
&\quad + D_{\alpha\beta\gamma} \delta_{\alpha\lambda} u_{2\beta,1} \delta u_{2\lambda,2} \\
&\quad + D_{\alpha\beta\gamma} \delta_{\alpha\lambda} u_{3\beta,2} \delta u_{3\lambda,1} + D_{\alpha\beta\gamma} \delta_{\alpha\lambda} u_{3\beta,1} \delta u_{3\lambda,2} \\
&= D_{\lambda\beta\gamma} \left[u_{1\beta,2} \delta u_{1\lambda,1} + \left(\delta_{\beta 0} + u_{1\beta,1}\right) \delta u_{1\lambda,2} \right. \\
&\quad + \left(\delta_{\beta 0} + u_{2\beta,2}\right) \delta u_{2\lambda,1} + u_{2\beta,1} \delta u_{2\lambda,2} \\
&\quad \left. + u_{3\beta,2} \delta u_{3\lambda,1} + u_{3\beta,1} \delta u_{3\lambda,2} \right]
\end{aligned} \tag{146}$$

$$\begin{aligned}
\delta\kappa_{11\gamma} &= \frac{\partial \kappa_{11\gamma}}{\partial \beta_{1\lambda,1}} \delta \beta_{1\lambda,1} \\
&= \delta_{\gamma\lambda} \delta \beta_{1\lambda,1} = D_{\lambda\beta\gamma} \delta_{\beta 0} \delta \beta_{1\lambda,1}
\end{aligned} \tag{147}$$

$$\begin{aligned}
\delta\kappa_{22\gamma} &= \frac{\partial \kappa_{22\gamma}}{\partial \beta_{2\lambda,2}} \delta \beta_{2\lambda,2} \\
&= \delta_{\gamma\lambda} \delta \beta_{2\lambda,2} = D_{\lambda\beta\gamma} \delta_{\beta 0} \delta \beta_{2\lambda,2}
\end{aligned} \tag{148}$$

$$\begin{aligned}
2\delta\kappa_{12\gamma} &= \frac{2\partial \kappa_{12\gamma}}{\partial \beta_{1\lambda,2}} \delta \beta_{1\lambda,2} + \frac{2\partial \kappa_{12\gamma}}{\partial \beta_{2\lambda,1}} \delta \beta_{2\lambda,1} \\
&= \delta_{\gamma\lambda} \delta \beta_{1\lambda,2} + \delta_{\gamma\lambda} \delta \beta_{2\lambda,1} \\
&= D_{\lambda\beta\gamma} \left(\delta_{\beta 0} \delta \beta_{1\lambda,2} + \delta_{\beta 0} \delta \beta_{2\lambda,1} \right)
\end{aligned} \tag{149}$$

$$\begin{aligned}
\delta\gamma_{13\gamma} &= \frac{\partial \gamma_{13\gamma}}{\partial \beta_{1\lambda}} \delta \beta_{1\lambda} + \frac{\partial \gamma_{13\gamma}}{\partial u_{3\lambda,1}} \delta u_{3\lambda,1} \\
&= \delta_{\gamma\lambda} \delta \beta_{1\lambda} + \delta_{\gamma\lambda} \delta u_{3\lambda,1} \\
&= D_{\lambda\beta\gamma} \left(\delta_{\beta 0} \delta \beta_{1\lambda} + \delta_{\beta 0} \delta u_{3\lambda,1} \right)
\end{aligned} \tag{150}$$

$$\begin{aligned}
\delta\gamma_{23\gamma} &= \frac{\partial \gamma_{23\gamma}}{\partial \beta_{2\lambda}} \delta \beta_{2\lambda} + \frac{\partial \gamma_{23\gamma}}{\partial u_{3\lambda,2}} \delta u_{3\lambda,2} \\
&= \delta_{\gamma\lambda} \delta \beta_{2\lambda} + \delta_{\gamma\lambda} \delta u_{3\lambda,2} \\
&= D_{\lambda\beta\gamma} \left(\delta_{\beta 0} \delta \beta_{2\lambda} + \delta_{\beta 0} \delta u_{3\lambda,2} \right)
\end{aligned} \tag{151}$$

G Linearization of virtual shell strains

This section shows the detailed derivation of the linearization of the virtual shell strains.

$$\begin{aligned}\Delta\delta\varepsilon_{22\gamma} &= \frac{\partial\delta\varepsilon_{22\gamma}}{\partial u_{1\mu,2}}\Delta u_{1\mu,2} + \frac{\partial\delta\varepsilon_{22\gamma}}{\partial u_{2\mu,2}}\Delta u_{2\mu,2} + \frac{\partial\delta\varepsilon_{22\gamma}}{\partial u_{3\mu,2}}\Delta u_{3\mu,2} \\ &= D_{\lambda\beta\gamma}\delta_{\beta\mu}\left[\delta u_{1\lambda,2}\Delta u_{1\mu,2} + \delta u_{2\lambda,2}\Delta u_{2\mu,2} \right. \\ &\quad \left. + \delta u_{3\lambda,2}\Delta u_{3\mu,2}\right] \\ &= D_{\lambda\mu\gamma}\left[\delta u_{1\lambda,2}\Delta u_{1\mu,2} + \delta u_{2\lambda,2}\Delta u_{2\mu,2} \right. \\ &\quad \left. + \delta u_{3\lambda,2}\Delta u_{3\mu,2}\right] \end{aligned} \tag{152}$$

$$\begin{aligned}2\Delta\delta\varepsilon_{12\gamma} &= \frac{2\partial\delta\varepsilon_{12\gamma}}{\partial u_{1\mu,1}}\Delta u_{1\mu,1} + \frac{2\partial\delta\varepsilon_{12\gamma}}{\partial u_{1\mu,2}}\Delta u_{1\mu,2} \\ &\quad + \frac{2\partial\delta\varepsilon_{12\gamma}}{\partial u_{2\mu,1}}\Delta u_{2\mu,1} + \frac{2\partial\delta\varepsilon_{12\gamma}}{\partial u_{2\mu,2}}\Delta u_{2\mu,2} \\ &\quad + \frac{2\partial\delta\varepsilon_{12\gamma}}{\partial u_{3\mu,1}}\Delta u_{3\mu,1} + \frac{2\partial\delta\varepsilon_{12\gamma}}{\partial u_{3\mu,2}}\Delta u_{3\mu,2} \\ &= D_{\lambda\beta\gamma}\delta_{\beta\mu}\left[\delta u_{1\lambda,2}\Delta u_{1\mu,1} + \delta u_{1\lambda,1}\Delta u_{1\mu,2} \right. \\ &\quad + \delta u_{2\lambda,2}\Delta u_{2\mu,1} + \delta u_{2\lambda,1}\Delta u_{2\mu,2} \\ &\quad \left. + \delta u_{3\lambda,2}\Delta u_{3\mu,1} + \delta u_{3\lambda,1}\Delta u_{3\mu,2}\right] \\ &= D_{\lambda\mu\gamma}\left[\delta u_{1\lambda,2}\Delta u_{1\mu,1} + \delta u_{1\lambda,1}\Delta u_{1\mu,2} \right. \\ &\quad + \delta u_{2\lambda,2}\Delta u_{2\mu,1} + \delta u_{2\lambda,1}\Delta u_{2\mu,2} \\ &\quad \left. + \delta u_{3\lambda,2}\Delta u_{3\mu,1} + \delta u_{3\lambda,1}\Delta u_{3\mu,2}\right] \end{aligned} \tag{153}$$

H Stochastic discretization

This section illustrates the stochastic discretization of the stochastic weak form. The virtual work of the external loads can be reformulated to

$$\begin{aligned}&\mathbb{E}\left[\delta\pi_{ext}(\omega)\right] \\ &= \mathbb{E}\left[\int_{\Omega_0}\delta\mathbf{v}^T(\omega)\bar{\mathbf{q}}(\omega)\,\mathrm{d}A + \int_{\partial\Omega_0^\sigma}\delta\mathbf{v}^T(\omega)\bar{\mathbf{f}}(\omega)\,\mathrm{d}s\right] \\ &= \mathbb{E}\left[\int_{\Omega_0}\delta\mathbf{v}_\alpha^T\Psi_\alpha\bar{\mathbf{q}}_\beta\Psi_\beta\mathrm{d}A + \int_{\partial\Omega_0^\sigma}\delta\mathbf{v}_\alpha^T\Psi_\alpha\bar{\mathbf{f}}_\beta\Psi_\beta\mathrm{d}s\right] \\ &= \int_{\Omega_0}\delta\mathbf{v}_\alpha^T\bar{\mathbf{q}}_\beta\delta_{\alpha\beta}\mathrm{d}A + \int_{\partial\Omega_0^\sigma}\delta\mathbf{v}_\alpha^T\bar{\mathbf{f}}_\beta\delta_{\alpha\beta}\mathrm{d}s \\ &= \int_{\Omega_0}\delta\mathbf{v}_\alpha^T\bar{\mathbf{q}}_\alpha\mathrm{d}A + \int_{\partial\Omega_0^\sigma}\delta\mathbf{v}_\alpha^T\bar{\mathbf{f}}_\alpha\mathrm{d}s\,. \end{aligned} \tag{154}$$

Analogously, the virtual work of the internal forces is discretized

$$\begin{aligned}&\mathbb{E}\left[\delta\pi_i(\omega)\right] \\ &= \mathbb{E}\left[\int_{\Omega_0}\delta\boldsymbol{\varepsilon}^T(\omega)\boldsymbol{\sigma}(\omega)\mathrm{d}A\right] \\ &= \mathbb{E}\left[\int_{\Omega_0}\delta\boldsymbol{\varepsilon}_\alpha^T\Psi_\alpha\boldsymbol{\sigma}_\beta\Psi_\beta\mathrm{d}A\right] = \int_{\Omega_0}\delta\boldsymbol{\varepsilon}_\alpha^T\boldsymbol{\sigma}_\beta\delta_{\alpha\beta}\mathrm{d}A \\ &= \int_{\Omega_0}\delta\boldsymbol{\varepsilon}_\alpha^T\boldsymbol{\sigma}_\alpha\mathrm{d}A\,. \end{aligned} \tag{155}$$

The linearization of the residual is discretized in a similar way

$$\begin{aligned}&\mathbb{E}\left[\Delta\delta\pi(\omega)\right] \\ &= \mathbb{E}\left[\int_{\Omega_0}\delta\boldsymbol{\varepsilon}^T(\omega)\Delta\boldsymbol{\sigma}(\omega) + \Delta\delta\boldsymbol{\varepsilon}^T(\omega)\boldsymbol{\sigma}(\omega)\,\mathrm{d}A\right] \\ &= \mathbb{E}\left[\int_{\Omega_0}\delta\boldsymbol{\varepsilon}_\alpha^T\Psi_\alpha\,\mathbf{D}_\beta\Psi_\beta\,\Delta\boldsymbol{\varepsilon}_\gamma\Psi_\gamma + \Delta\delta\boldsymbol{\varepsilon}_\alpha^T\Psi_\alpha\,\boldsymbol{\sigma}_\beta\Psi_\beta\,\mathrm{d}A\right] \\ &= \int_{\Omega_0}\delta\boldsymbol{\varepsilon}_\alpha^T\,\mathbf{D}_\beta\,\Delta\boldsymbol{\varepsilon}_\gamma\,D_{\alpha\beta\gamma} + \Delta\delta\boldsymbol{\varepsilon}_\alpha^T\,\boldsymbol{\sigma}_\alpha\,\mathrm{d}A\,. \end{aligned} \tag{156}$$

I Local Cartesian basis and transformation

The local Cartesian basis is defined at the element center, which is given by

$$\tilde{\mathbf{X}}_0 := \frac{1}{4}\sum_{I=1}^{4}\tilde{\mathbf{X}}_I\,. \tag{157}$$

All quantities that refer to the global coordinate system $\mathbf{e}_i$ are designated with $\tilde{(\bullet)}$. Using the diagonal vectors in the shell plane, the local basis vectors $\mathbf{A}_i$ can be calculated as

$$\begin{aligned}&\bar{\mathbf{d}}_1 = \tilde{\mathbf{X}}_3 - \tilde{\mathbf{X}}_1, \quad \mathbf{d}_1 = \bar{\mathbf{d}}_1/||\bar{\mathbf{d}}_1|| \\ &\bar{\mathbf{d}}_2 = \tilde{\mathbf{X}}_2 - \tilde{\mathbf{X}}_4, \quad \mathbf{d}_2 = \bar{\mathbf{d}}_2/||\bar{\mathbf{d}}_2|| \\ &\mathbf{A}_1 = (\mathbf{d}_1 + \mathbf{d}_2)/||\mathbf{d}_1 + \mathbf{d}_2|| \\ &\mathbf{A}_2 = (\mathbf{d}_1 - \mathbf{d}_2)/||\mathbf{d}_1 - \mathbf{d}_2|| \\ &\mathbf{A}_3 = \mathbf{d}_1 \times \mathbf{d}_2\,. \end{aligned} \tag{158}$$

Finally, the transformation matrix is given by

$$\mathbf{T} := \mathbf{A}_i \otimes \mathbf{e}_j = \left[\mathbf{A}_1\ \mathbf{A}_2\ \mathbf{A}_3\right]^T \quad \mathbf{T} \in \mathbb{R}^{3\times3}\,, \tag{159}$$

which is used to transform the nodal coordinates and nodal displacements with

$$\mathbf{X}_I = \mathbf{T}\left(\tilde{\mathbf{X}}_I - \tilde{\mathbf{X}}_0\right) \quad I = 1, \ldots, 4$$
$$\mathbf{v}_{I\alpha} = \begin{bmatrix} \mathbf{u}_{I\alpha} \\ \boldsymbol{\beta}_{I\alpha} \end{bmatrix} = \begin{bmatrix} \mathbf{T}_{3\times3} & \mathbf{0}_{3\times3} \\ \mathbf{0}_{3\times3} & \mathbf{T}_{3\times3} \end{bmatrix} \tilde{\mathbf{v}}_{I\alpha}$$
$$= \bar{\mathbf{T}}\,\tilde{\mathbf{v}}_{I\alpha} \quad \forall \alpha \in [0 \ldots P] \ . \tag{160}$$

The coefficient of the nodal displacement vector according to the global basis is given by

$$\tilde{\mathbf{v}}_{I\alpha} = \left[\tilde{u}_{1I\alpha},\, \tilde{u}_{2I\alpha},\, \tilde{u}_{3I\alpha},\, \tilde{\beta}_{1I\alpha},\, \tilde{\beta}_{2I\alpha},\, \tilde{\beta}_{3I\alpha}\right]^T \ . \tag{161}$$

At the element level, the residual and the tangent stiffness matrix can be mapped to the global basis with

$$\tilde{\mathbf{g}}^e_I = \bar{\mathbf{T}}^T \mathbf{g}^e_I \ , \qquad \tilde{\mathbf{k}}^e_{TIK} = \bar{\mathbf{T}}^T \mathbf{k}^e_{TIK}\, \bar{\mathbf{T}} \ . \tag{162}$$

J Transverse shear strain

In the context of the stochastic formulation, the compatible shear strains for the quadrilateral shell element are given by

$$\begin{aligned}\tilde{\gamma}_{\xi 3\gamma} = \frac{1}{4}(1-\eta)\Big[&x_1,_\xi^B \left(\beta_{11\gamma} + \beta_{12\gamma}\right) \\ &+ x_2,_\xi^B \left(\beta_{21\gamma} + \beta_{22\gamma}\right) + \left(u_{32\gamma} - u_{31\gamma}\right)\Big] \\ &+ \frac{1}{4}(1+\eta)\Big[x_1,_\xi^D \left(\beta_{13\gamma} + \beta_{14\gamma}\right) \\ &+ x_2,_\xi^D \left(\beta_{23\gamma} + \beta_{24\gamma}\right) + \left(u_{33\gamma} - u_{34\gamma}\right)\Big]\end{aligned} \tag{163}$$

and

$$\begin{aligned}\tilde{\gamma}_{\eta 3\gamma} = \frac{1}{4}(1-\xi)\Big[&x_1,_\eta^A \left(\beta_{14\gamma} + \beta_{11\gamma}\right) \\ &+ x_2,_\eta^A \left(\beta_{24\gamma} + \beta_{21\gamma}\right) + \left(u_{34\gamma} - u_{31\gamma}\right)\Big] \\ &+ \frac{1}{4}(1+\xi)\Big[x_1,_\eta^C \left(\beta_{12\gamma} + \beta_{13\gamma}\right) \\ &+ x_2,_\eta^C \left(\beta_{22\gamma} + \beta_{23\gamma}\right) + \left(u_{33\gamma} - u_{32\gamma}\right)\Big] \ .\end{aligned} \tag{164}$$

Within the bi-linear interpolation, the local derivatives of the coordinates can be specified as

$$\begin{aligned} x_1,_\eta^A &= \frac{1}{2}(x_{14} - x_{11}) \ , & x_2,_\eta^A &= \frac{1}{2}(x_{24} - x_{21}) \ , \\ x_1,_\xi^B &= \frac{1}{2}(x_{12} - x_{11}) \ , & x_2,_\xi^B &= \frac{1}{2}(x_{22} - x_{21}) \ , \\ x_1,_\eta^C &= \frac{1}{2}(x_{13} - x_{12}) \ , & x_2,_\eta^C &= \frac{1}{2}(x_{23} - x_{22}) \ , \\ x_1,_\xi^D &= \frac{1}{2}(x_{13} - x_{14}) \ , & x_2,_\xi^D &= \frac{1}{2}(x_{23} - x_{24}) \ . \end{aligned} \tag{165}$$

The variation of the modified shear strains are determined as

$$\begin{aligned}\delta\tilde{\gamma}_{\xi 3\gamma} = D_{\lambda\beta\gamma}\,\delta_{\beta 0}\Big\{&\frac{1}{4}(1-\eta)\Big[x_1,_\xi^B \left(\delta\beta_{11\lambda} + \delta\beta_{12\lambda}\right) \\ &+ x_2,_\xi^B \left(\delta\beta_{21\lambda} + \delta\beta_{22\lambda}\right) + \left(\delta u_{32\lambda} - \delta u_{31\lambda}\right)\Big] \\ &+ \frac{1}{4}(1+\eta)\Big[x_1,_\xi^D \left(\delta\beta_{13\lambda} + \delta\beta_{14\lambda}\right) \\ &+ x_2,_\xi^D \left(\delta\beta_{23\lambda} + \delta\beta_{24\lambda}\right) + \left(\delta u_{33\lambda} - \delta u_{34\lambda}\right)\Big]\Big\}\end{aligned} \tag{166}$$

and

$$\begin{aligned}\delta\tilde{\gamma}_{\eta 3\gamma} = D_{\lambda\beta\gamma}\,\delta_{\beta 0}\Big\{&\frac{1}{4}(1-\xi)\Big[x_1,_\eta^A \left(\delta\beta_{14\lambda} + \delta\beta_{11\lambda}\right) \\ &+ x_2,_\eta^A \left(\delta\beta_{24\lambda} + \delta\beta_{21\lambda}\right) + \left(\delta u_{34\lambda} - \delta u_{31\lambda}\right)\Big] \\ &+ \frac{1}{4}(1+\xi)\Big[x_1,_\eta^C \left(\delta\beta_{12\lambda} + \delta\beta_{13\lambda}\right) \\ &+ x_2,_\eta^C \left(\delta\beta_{22\lambda} + \delta\beta_{23\lambda}\right) + \left(\delta u_{33\lambda} - \delta u_{32\lambda}\right)\Big]\Big\} \ .\end{aligned} \tag{167}$$

Based on this notation, the modified **B**-matrix in Eq. (103) for the shear strains is derived.

Funding Open Access funding enabled and organized by Projekt DEAL.

References

1. Caflisch RE (1998) Monte Carlo and quasi-monte Carlo methods. Acta Numer 7:1–49. https://doi.org/10.1017/S0962492900002804
2. Ghanem RG, Spanos PD (1991) Stochastic finite elements: a spectral approach. Springer, New York
3. Wiener N (1938) The homogeneous chaos. Am J Math 60(4):897. https://doi.org/10.2307/2371268
4. Xiu D, Karniadakis GE (2002) The Wiener-Askey polynomial chaos for stochastic differential equations. SIAM J Sci Comput 24(2):619–644. https://doi.org/10.1137/S1064827501387826
5. Xiu D, Karniadakis GE (2003) Modeling uncertainty in flow simulations via generalized polynomial chaos. J Comput Phys 187(1):137–167. https://doi.org/10.1016/S0021-9991(03)00092-5
6. Efron B, Hastie T, Johnstone I, Tibshirani R (2004) Least angle regression. Annals Stat. https://doi.org/10.1214/009053604000000067
7. Blatman G, Sudret B (2010) An adaptive algorithm to build up sparse polynomial chaos expansions for stochastic finite ele-

ment analysis. Probab Eng Mech 25(2):183–197. https://doi.org/10.1016/j.probengmech.2009.10.003
8. Blatman G, Sudret B (2011) Adaptive sparse polynomial chaos expansion based on least angle regression. J Comput Phys 230(6):2345–2367. https://doi.org/10.1016/j.jcp.2010.12.021
9. Debusschere BJ, Najm HN, Pébay PP, Knio OM, Ghanem RG, Le Maitre OP (2004) Numerical challenges in the use of polynomial chaos representations for stochastic processes. SIAM J Sci Comput 26(2):698–719. https://doi.org/10.1137/S1064827503427741
10. Ghanem R (1999) Ingredients for a general purpose stochastic finite elements implementation. Comput Methods Appl Mech Eng 168(1–4):19–34. https://doi.org/10.1016/S0045-7825(98)00106-6
11. Sudret B, Der Kiureghian A (2000) Stochastic finite element methods and reliability –a state-of-the-art report. University of California, Berkeley, Department of Civil and Environmental Engineering
12. Eiermann M, Ernst OG, Ullmann E (2007) Computational aspects of the stochastic finite element method. Comput Vis Sci 10(1):3–15. https://doi.org/10.1007/s00791-006-0047-4
13. Stefanou G (2009) The stochastic finite element method: Past, present and future. Comput Methods Appl Mech Eng 198(9–12):1031–1051. https://doi.org/10.1016/j.cma.2008.11.007
14. Arregui-Mena JD, Margetts L, Mummery PM (2014) Practical application of the stochastic finite element method. Arch Comput Methods Eng 23(1):171–190. https://doi.org/10.1007/s11831-014-9139-3
15. Pellissetti M, Schuëller G (2006) On general purpose software in structural reliability–an overview. Struct Saf 28(1–2):3–16. https://doi.org/10.1016/j.strusafe.2005.03.004
16. Ghanem R (1999) Higher-order sensitivity of heat conduction problems to random data using the spectral stochastic finite element method. J Heat Transf 121(2):290–299. https://doi.org/10.1115/1.2825979
17. Xiu D, Karniadakis GE (2003) A new stochastic approach to transient heat conduction modeling with uncertainty. Int J Heat Mass Transf 46(24):4681–4693. https://doi.org/10.1016/S0017-9310(03)00299-0
18. Ghanem R (1998) Probabilistic characterization of transport in heterogeneous media. Comput Methods Appl Mech Eng 158(3–4):199–220. https://doi.org/10.1016/S0045-7825(97)00250-8
19. Sarkar A, Ghanem R (2002) Mid-frequency structural dynamics with parameter uncertainty. Comput Methods Appl Mech Eng 191(47–48):5499–5513. https://doi.org/10.1016/S0045-7825(02)00465-6
20. Xiu D, Em Karniadakis G (2002) Modeling uncertainty in steady state diffusion problems via generalized polynomial chaos. Comput Methods Appl Mech Eng 191(43):4927–4948. https://doi.org/10.1016/S0045-7825(02)00421-8
21. Chung DB, Gutiérrez MA, Remmers J, Borst R (2004) Stochastic finite element modelling of fibre-metal laminates. In: 45th AIAA/ASME/ASCE/AHS/ASC Structures, Structural Dynamics; Materials Conference, American Institute of Aeronautics and Astronautics, https://doi.org/10.2514/6.2004-1992
22. Chung DB, Gutiérrez MA, Borst R (2005) Object-oriented stochastic finite element analysis of fibre-metal laminates. Comput Methods Appl Mech Eng 194(12–16):1427–1446. https://doi.org/10.1016/j.cma.2004.03.021
23. Stefanou G, Papadrakakis M (2004) Stochastic finite element analysis of shells with combined random material and geometric properties. Comput Methods Appl Mech Eng 193(1–2):139–160. https://doi.org/10.1016/j.cma.2003.10.001
24. Anders M, Hori M (2001) Three-dimensional stochastic finite element method for elasto-plastic bodies. Int J Numer Meth Eng 51(4):449–478. https://doi.org/10.1002/nme.165
25. Rosic BV, Matthies HG (2011) Stochastic Galerkin method for the Elastoplasticity problem with uncertain parameters. Springer, Berlin Heidelberg, pp 303–310
26. Rosic BV, Matthies HG (2014) Variational theory and computations in stochastic plasticity. Arch Comput Methods Eng 22(3):457–509. https://doi.org/10.1007/s11831-014-9116-x
27. Sett K, Jeremić B, Levent Kavvas M (2011) Stochastic elastic–plastic finite elements. Comput Methods Appl Mech Eng 200(9–12):997–1007. https://doi.org/10.1016/j.cma.2010.11.021
28. Acharjee S, Zabaras N (2006) Uncertainty propagation in finite deformations–a spectral stochastic Lagrangian approach. Comput Methods Appl Mech Eng 195(19–22):2289–2312. https://doi.org/10.1016/j.cma.2005.05.005
29. Papadopoulos V, Kalogeris I, Giovanis DG (2019) A spectral stochastic formulation for nonlinear framed structures. Probab Eng Mech 55:90–101. https://doi.org/10.1016/j.probengmech.2018.11.002
30. Ammouche Y, Jérusalem A (2022) A modular nonlinear stochastic finite element formulation for uncertainty estimation. Comput Methods Appl Mech Eng 396:115044. https://doi.org/10.1016/j.cma.2022.115044
31. Bathe K, Dvorkin EN (1985) A four-node plate bending element based on mindlin/reissner plate theory and a mixed interpolation. Int J Numer Meth Eng 21(2):367–383. https://doi.org/10.1002/nme.1620210213
32. Dvorkin EN, Bathe K (1984) A continuum mechanics based four-node shell element for general non-linear analysis. Eng Comput 1(1):77–88. https://doi.org/10.1108/eb023562
33. Gruttmann F, Wagner W (2005) A linear quadrilateral shell element with fast stiffness computation. Comput Methods Appl Mech Eng 194(39–41):4279–4300. https://doi.org/10.1016/j.cma.2004.11.005
34. Wagner W, Gruttmann F (2005) A robust non-linear mixed hybrid quadrilateral shell element. Int J Numer Meth Eng 64(5):635–666. https://doi.org/10.1002/nme.1387
35. Wagner W, Gruttmann F (1994) A simple finite rotation formulation for composite shell elements. Eng Comput 11(2):145–176. https://doi.org/10.1108/02644409410799209
36. Oñate E (2013) Structural analysis with the finite element method linear statics. Springer, Netherlands. https://doi.org/10.1007/978-1-4020-8743-1
37. Soize C, Ghanem R (2004) Physical systems with random uncertainties: Chaos representations with arbitrary probability measure. SIAM J Sci Comput 26(2):395–410. https://doi.org/10.1137/S1064827503424505
38. Sobol I (2001) Global sensitivity indices for nonlinear mathematical models and their monte Carlo estimates. Math Comput Simul 55(1–3):271–280. https://doi.org/10.1016/S0378-4754(00)00270-6
39. Sudret B (2008) Global sensitivity analysis using polynomial chaos expansions. Reliab Eng Syst Saf 93(7):964–979. https://doi.org/10.1016/j.ress.2007.04.002
40. Taylor RL (2024) FEAP - finite element analysis program. University of California, Berkeley http://projects.ce.berkeley.edu/feap/
41. Yeom CH, Lee SW (1989) An assumed strain finite element model for large deflection composite shells. Int J Numer Meth Eng 28(8):1749–1768. https://doi.org/10.1002/nme.1620280804
42. Gruttmann F, Wagner W (2013) A coupled two-scale shell model with applications to layered structures. Int J Numer Meth Eng 94(13):1233–1254. https://doi.org/10.1002/nme.4496
43. Jarzebski P, Wisniewski K, Taylor RL (2015) On parallelization of the loop over elements in FEAP. Comput Mech 56(1):77–86. https://doi.org/10.1007/s00466-015-1156-z
44. Sudret B (2014) Polynomial chaos expansions and stochastic finite element methods vol 6, RC Press: Chap, pp 65–300

45. Field RV Jr, Grigoriu M (2007) Convergence properties of polynomial chaos approximations for l2 random variables. https://doi.org/10.2172/903430
46. Adams JC (1878) On the expression of the product of any two legendre's coefficients by means of a series of legendre's coefficients. Proc R Soc Lond. https://doi.org/10.1098/rspl.1878.0016